

Feedback Control of an Exoskeleton for Paraplegics

Toward Robustly Stable Hands-free Dynamic Walking

Omar Harib, Ayonga Hereid, Ayush Agrawal, Thomas Gurriet,
Sylvain Finet, Guilhem Boeris, Alexis Duburcq, M. Eva Mungai,
Matthieu Masselin, Aaron D. Ames, Koushil Sreenath, Jessy Grizzle

POC: O. Harib(oharib@umich.edu)

February 4, 2018

“I will never forget the emotion of my first steps [...],” Françoise, first user during initial trials of the exoskeleton ATALANTE [1] discussed in this paper. “I am tall again!”, Sandy, the fourth user after standing up in the exoskeleton. In these early tests, complete paraplegic patients have dynamically walked up to 10 m without crutches or other assistance using a feedback control method originally invented for bipedal robots. This paper describes the hardware, shown in Figure 1, that has been designed to achieve hands-free dynamic walking, the control laws that have been deployed and those being developed to provide enhanced mobility and robustness, as well as the early test results alluded to above. **In this paper, dynamic walking refers to a motion that is orbitally stable as opposed to statically stable.**

Across the world, 70 million walking-impaired people have one life objective: to walk again. At present approximately 4.7 million people in the United States would benefit from an active lower-limb exoskeleton due to the effects of stroke, polio, multiple sclerosis, spinal cord injury, and cerebral palsy [2]. Moreover, by 2050, an estimated 1.5 million people in the United States will be living with a major lower-limb amputation [3]. Such individuals expend up to twice the metabolic effort to walk at half the speed of able-bodied persons, experience higher-risk of falls, and have secondary pathological conditions such as osteoarthritis, back pain, and depression [4]–[6]. Lower-limb exoskeletons serve as assistive devices by providing support and balance to wheelchair users and enabling them to perform normal ambulatory functions such as standing, walking and climbing stairs. Lower-limb exoskeletons have also been utilized for gait training and rehabilitation purposes.

More importantly, standing and walking with these assistive devices provides exceptional health benefits. For instance, for paraplegics the benefits include improvement of blood

circulation, of respiratory, urinary, and intestinal functions, as well as positive psychological effects [7], fundamentally improving their quality of life. For spinal cord injury (SCI) patients, the benefits include improved bone density, cardiorespiratory function, gastrointestinal function, sitting balance, and decreased pain and spasticity [8]. ~~It is thus our moral job to enable these people to stand and walk.~~

The objective of the work described herein is to translate formal control design methodologies from bipedal robots to exoskeleton systems so as to achieve dynamic hands-free walking. This is a challenging problem as control of bio-mechatronic exoskeleton devices not only share many of the challenges of bipedal robot locomotion but also challenges introduced by the integration of an active human user. These challenges include, nonlinear, high degree-of-freedom hybrid dynamics, workspace limitations, actuator constraints, unilateral ground contact forces, being robust to variations in the user's dynamical parameters such as mass and inertia, being able to handle interaction forces between the user and the device, and enforcing safety-critical constraints for safe operation of the exoskeleton.

Over the years, several research groups and companies have begun responding to the need and benefits of exoskeletons. Exoskeletons can be designed for human performance augmentation and as orthotic devices. Exoskeletons for Human Performance Augmentation are designed to enhance the strength and physical capabilities of able-bodied users, to provide fatigue relief and protection to factory and construction workers, soldiers, and disaster relief workers, and to assist them in carrying heavy loads for prolonged periods of time. In contrast, orthotic devices are designed to assist and restore autonomy to individuals with physical impairments causing difficulty in walking. Orthotic devices are also designed for rehabilitation purposes - to provide gait training and therapy. A comprehensive review of the state-of-the art lower-limb exoskeletons can be found in [9]–[11].

Early exoskeletons, developed by General Electric [12], the University of Wisconsin [13], and the Mihailo Pupin Institute [14], [15], focused on human augmentation or assistance, supporting multi-task capabilities such as walking, standing up from a seated position, sitting down, stepping over obstacles, and climbing stairs, all through pre-programmed motion patterns that were executed at the user's command. These systems, however, were not very robust. Turning to more recent devices, Ekso Bionics' robotic exoskeleton EksoGT [16] is primarily designed for use in clinical settings for rehabilitation and gait training for stroke and SCI patients. ReWalk [17], [18] is another robotic lower-limb exoskeleton to enable patients with SCI to stand-up, walk, turn and climb stairs. The Hybrid Assistive Limb (HAL) [19] developed at the University of Tsukuba, Japan and Cyberdyne [20] provides locomotion assistance to physically challenged persons. These are high-degree-of-freedom exoskeletons that have multiple actuators

at the hip, knee and ankle. A primary limitation, however, of the cited exoskeletons is that they
2 require external support mechanisms such as crutches or canes for the user to maintain balance
3 while walking with the device. While REX bionics' lower-limb exoskeleton provides hands-free
4 functionality, it only allows slow static gaits with velocities on the order of 0.05 m/s.

While modern day hardware for exoskeletons and prosthetics is becoming lighter, stronger,
6 and power-dense, the current approaches to control of powered leg devices are rudimentary and
driven by finite-state machines with several phases such as swing, stance, heel-strike and toe-
8 off [21], [22, Fig. 9], each with numerous tunable parameters that are specific to each user
[23], [24], offering no formal guarantees of either stability or safety [25], and typically require
10 the use of additional aids such as crutches to be safely used [26], [27]. A general review of
various control strategies for lower limb assistive robotics is presented in [21], [28], [29]. In
12 particular, low-level control strategies are either position-based [30]–[34] or torque / force-based
[35]–[39], while a higher-level impedance or admittance controller is used to regulate human-
14 device interaction forces. This is in stark contrast to the surge in control technology for highly
dynamic bipedal locomotion [40]–[45], where tools are being developed that allow rapid design
16 of gaits and model-based feedback controllers, that respect physical constraints of the system
such as torque limits and joint speeds, while providing formal guarantees on stability, safety
18 and robustness to uncertainties in the model and in the environment [46]–[50]. If the control
and design methodologies underlying advanced locomotion strategies for bipedal robots can be
20 successfully translated to powered prostheses and exoskeletons in a holistic and formal manner,
the end result promises to be a new generation of wearable robotic devices that deliver the next
22 level of stable, safe, and efficient mobility.

A new paradigm of control design is thus necessary to achieve dynamic hands-free
24 exoskeleton walking, one that transcends current approaches involving state machines and
extensive gain tuning [51]–[54]. The heart of our approach involves virtual constraints and
26 hybrid invariant manifolds. Virtual constraints are functional relations achieved on the generalized
coordinates of the exoskeleton via feedback control; they provide a systematic means for
28 coordinating limb motion and providing corrective actions to attenuate disturbances, without
resorting to low-dimensional pendulum models. Indeed, the virtual constraints are designed
30 herein on the basis of the 18 degree-of-freedom floating-base model of the exoskeleton and
offline trajectory optimization. This approach is validated both numerically and in pre-clinical
32 experimental testing, the latter enabling paraplegics to walk hands-free, with all control actions
required for stable dynamic walking provided by an onboard controller. We also present a recent
34 generalization of virtual constraints that is based on a unique combination a fast offline trajectory
optimization and machine learning, in tandem with online robust trajectory tracking. These newer

techniques harness the power of modern optimization tools and are blazing the way for improved controller designs that deliver multiple walking speeds, turning, and enhanced robustness for exoskeleton locomotion.

In the remainder of the paper, we introduce the exoskeleton mechanism under study, construct a dynamic model for control design, and develop control objectives for achieving hands-free dynamic walking. Following this, state-of-the-art techniques in bipedal control are summarized and how to translate a method based on virtual constraints to exoskeletons is highlighted. A generalization of virtual constraints is presented that combines offline trajectory optimization and machine learning to design stabilized gaits that can be robustly tracked online. Both control design approaches are illustrated in simulation, while pre-clinical tests are currently available only for the first method. In these [early](#) tests, [aimed at evaluating the viability of the hardware and the approaches to control design discussed in the current paper, fully](#) paraplegic patients are able to dynamically walk hands-free. [To be clear, these tests are not aimed at assessing patient outcomes.](#)

To be totally transparent, in terms of “gain tuning”, the local controllers at the joint level will be tuned based on a nominal walking motion and then left fixed. In early stages of optimization, the constraints are adjusted to provide adequate foot clearances given the observed tracking errors in the local joint controllers and small errors in calibration. Post-optimization, a constant bias is sometimes added to a commanded joint profile to compensate for model errors or tracking errors.

The Exoskeleton and Its Dynamic Model

In this section, we first provide a brief description of the hardware and sensors of the exoskeleton hardware. We next derive a mathematical model of walking for the human-exoskeleton system, which can be represented by a hybrid control system. The model developed here is later used to find periodic walking gaits, develop feedback controllers to stabilize these gaits, and perform numerical simulations of the hybrid control system. The most basic of these generated gaits are evaluated in experiments.

Hardware Description

ATALANTE, developed by the French startup Wandercraft, is a fully-actuated lower-limb exoskeleton intended for use in medical centers for rehabilitation of patients with paraplegia. The exoskeleton consists of 12 actuated joints as shown in Figure 2: three joints that control the spherical motion of each hip, and in each leg, a single joint for the knee, and two joints for the

ankle rotation in the sagittal and frontal plane, respectively. Except for the ankle, where a special
2 mechanism is mounted, each degree of freedom is independently actuated by a brushless DC
3 motor. The displacement and velocity of each actuated joint are measured by a digital encoder
4 mounted on the corresponding motor as well as by three Inertial Measurement Units (IMUs),
5 with one attached to the torso and one on each leg [above the ankles](#). Four 3-axis force sensors
6 attached to the bottom of each foot are used to detect ground contact. All electrical components
7 of the exoskeleton are controlled by a central processing unit running a real-time operating
8 system and in charge of high-level computations.

The mechanical design of ATALANTE allows the leg length and hip width to be manually
10 adjusted to fit to an individual patient's personal measurements. This presents a challenge from
11 the control design perspective in that the controller should be robust to these physical changes
12 of the model. Because the exoskeleton is designed to fully support the user's weight, the user
13 is securely strapped to the device from the feet up to the abdomen as shown in Figure 2.

14 Mathematical Representation

With a goal to study the dynamical behavior of the human-exoskeleton and to avoid over
16 complicating the model by considering the compliant elements present in the human body and
17 exoskeleton linkages, the lumped human-exoskeleton system is modeled as a rigid body system
18 represented by a kinematic tree as shown in Figure 2. Different from the previous work in [53],
19 in which an articulated model of the human torso is considered to control the behavior of the
20 exoskeleton via the user's upper body posture, in this article, the upper body of the human is
21 modeled as a single rigid link attached to the torso of the exoskeleton. In particular, the patient
22 does not provide any actuation, however, the approximate masses and inertias of the patient are
23 combined in the corresponding links of the exoskeleton. Such a model appears to be appropriate
24 for paraplegic patients who have complete loss of motor input in their lower extremity.

Based on the rigid body assumption, the mathematical representation of the system
dynamics can be obtained via the Euler-Lagrangian equations of motion of rigid body dynamics.
Specifically, a floating-base generalized coordinate system is considered with the coordinate
variables defined as

$$q = (p, \phi, q_b) \in \mathcal{Q}, \quad (1)$$

where $p \in \mathbb{R}^3$ and $\phi \in SO(3)$ denote the relative position and orientation of the exoskeleton's
26 base frame with respect to the world frame respectively, and $q_b \in \mathbb{R}^{12}$ denotes the relative angles
of the actuated joints.

This article considers a simplified gait corresponding to flat-footed walking. Specifically,

the gait consists of alternating phases of a continuous, single support *swing phase* and an instantaneous, double support *impact phase*, with the stance foot maintained flat on the ground at all times (i.e., the stance foot is not allowed to roll or slip) and the swing foot parallel to the ground at foot strike and foot lift-off. As is common practice in the control design of legged robots [55], [56], the ground contact with the stance foot is considered as non-compliant. Hence, under this assumption, the ground contact can be modeled as a *holonomic constraint*, which enforces the position and orientation of the stance foot to remain constant throughout the swing phase. The dynamical equations of the swing phase with stance foot contact can be obtained as

$$D(q)\ddot{q} + C(q, \dot{q})\dot{q} + G(q) = Bu + J_{st}^T(q)F_{st}, \quad (2)$$

where D, C, G are the inertia, Coriolis, and gravity matrices respectively that are obtained directly from the exoskeleton's Universal Robot Description File (URDF) [57] using FROST [58], an open-source MATLAB toolkit for modeling, trajectory optimization and simulation of hybrid dynamical systems. The Jacobian J_{st} of the holonomic constraint and the ground contact wrench $F_{st} \in \mathbb{R}^6$ enforces the holonomic constraint of the the stance foot being flat on the ground [56].

We note in passing that the presented model is a floating-base model. An equivalent pinned-foot model can be developed where the stance foot wrench does not explicitly appear in the dynamic equations. “Pinned versus Floating base models” presents the advantages of one over the other.

Further, under the rigid ground assumption, the swing foot impact with the ground will be considered as plastic (coefficient of restitution is zero) and instantaneous (the impact forces and moments act over an infinitesimal interval of time) impact. During an impact, the coordinate variables of the system remain unchanged. However, the generalized velocities \dot{q} undergo a discrete jump due to the instantaneous change in the generalized momentum. This is captured by a *reset map* Δ which represents the relationship between the pre-impact states x^- with the post-impact states x^+ . Let $x = (q, \dot{q}) \in T\mathcal{Q}$ be the states of the system dynamics, where $T\mathcal{Q}$ is the tangent space of \mathcal{Q} , the hybrid system model of the flat-footed walking of the exoskeleton can be written as

$$\Sigma : \begin{cases} \dot{x} = f(x) + g(x)u, & x \notin S, \\ x^+ = \Delta(x^-), & x \in S. \end{cases} \quad (3)$$

where S is the guard or switching surface which determines the specific condition (i.e., the swing foot impacting the ground) that triggers the discrete events and the vector fields f, g are from the continuous-time swing-phase dynamics in (2). See [56] for a thorough discussion on obtaining dynamical models for bipedal mechanical systems.

Gait Objectives, Important Constraints, and Controller Architecture

2 The embedded control system needs to generate comfortable, robustly stable walking gaits
3 that respect mechanical limits of the exoskeleton, such as joint and torque limits, initiate smooth
4 (not jarring) foot contact with the ground, and satisfy ground contact constraints that avoid
5 slipping. These requirements will be the main focus of the paper. In previous work [53], we
6 provided additional features in the closed-loop system that may provide an intuitive means for
7 the user to regulate walking speed, and eventually, direction.

8 Gait Design Objectives

10 The gaits designed in this paper are destined for testing in a medical facility where an
11 engineer or therapist will provide external commands for walking speed. A wearer’s directional-
12 and-speed-control interface will be tested at a later stage. Gaits will be designed here for walking
13 in a straight line at speeds that vary from -0.3 m/s to 0.3 m/s. For comparison purposes, the
14 relaxed human walking gait is approximately 0.9 m/s.

14 The time duration of a step will be set to 0.7 s. Our observation is that shorter step times
15 closer to 0.5 s, while easier to stabilize, are uncomfortable for the user. To limit the transmission
16 of vibrations from the exoskeleton to the user, the impact of the swing foot with the ground
17 needs to be carefully regulated. Just before impact, we try to achieve near-zero forward and
18 lateral velocities of the foot with respect to the ground, while the downward velocity of the foot
19 is between -0.1 and -0.3 m/s. The upper bound ensures a transversal intersection of the foot
20 with the ground, a key guard condition in the hybrid controller, while the lower bound is for
21 user comfort.

22 It is desirable for the user to be able to maintain an upright posture when using the
23 exoskeleton to limit demands on abdominal and dorsal muscles, which may have been weakened
24 through prolonged use of a wheelchair. We have settled on left-right swaying motions that are
25 less than two degrees, and a forward lean angle that is between two and six degrees. For user
26 safety, the knee angles are bounded above five degrees away from straight and the ankles are
27 limited to ± 23 degrees. [Joint safety limits are imposed through a combination of hardware limits](#)
28 [and software enforced limits](#).

Ground Contact.

The holonomic constraints for modeling ground are taken from [56]. The key things to note are that the ground cannot pull on a foot and a “friction cone” must be respected to avoid

foot slippage, namely,

$$F_z > 0, \quad (4)$$

$$F_x^2 + F_y^2 \leq \mu^2 F_z^2, \quad (5)$$

where, $[F_x, F_y, F_z]$ is a vector of ground reaction forces acting on the stance foot, as shown in Figure 3, and $0 < \mu < 1$ is the coefficient of friction.

For the gaits used in this study, we will simplify the motions of the exoskeleton by imposing that the stance foot remains flat on the ground. As explained in [56], this requires moment constraints so that that foot does not roll about one of its axes. The stance width is set at 27 cm. This relatively wide stance limits rolling about the outer edge of the stance foot, which is typically harder to recover from than rolling inwards on the stance foot, while also promoting lateral stability. To provide additional robustness against foot rotation, we design the gaits so that the Zero Moment Point (ZMP) lies in the shaded areas shown in Figure 3; though it is not exactly the same thing, for the purpose of this paper, the reader can think of the ZMP as being the Center of Pressure (CoP) of the forces distributed on the sole of the foot. In addition, due to a heavy battery pack mounted just behind the user's hips, the center of mass of the exoskeleton is towards the heel of the foot when the leg is straight. Designing gaits with the ZMP towards the forward section of the foot prevents the exoskeleton from rolling backward on its stance foot. In our experience, rolling forward on the foot has not been a concern.

16 Other Objectives

To reduce the chance of the swing foot contacting the ground prematurely, gaits are designed with relatively large foot clearance in the middle of the step. The heel is designed to be 10 cm above the ground and the toe to be 5 cm above the ground. Larger foot clearance results in easier handling of terrain irregularities and trip recovery via foot placement. Potential downsides include greater torque requirements and motions that are closer to joint limits. Because flat walking is assumed, gaits need to be designed such that the feet are parallel to the ground during lift off and impact.

24 Controller Architecture

The overall control structure is shown in Figure 4. The Control Policy is responsible for specifying the evolution of key quantities of the exoskeleton, such as torso angle, swing leg angle (imagine a line from the hip to the ankle), and stance leg length (once again, a line from the hip to the ankle). These synthetic quantities are often more intuitive for the control engineer and the test engineer to use when specifying and discussing gait designs.

The Low-level Controller is responsible for associating the synthetic high-level quantities to the individual actuators of the exoskeleton. ~~When push comes to shove~~ During early testing, the simpler the low-level controller is, the easier it is to make rapid changes and uncover bugs.

4 The low-level joint controllers assure trajectory tracking with less than two degrees of error. The main task to be discussed later in the paper is therefore the association of high-level control

6 policy objectives to individual (or pairs of) joints and motors.

As its name suggests, the Guard Checker monitors quantities associated with events in a gait. In the real world, leg swapping is a control decision and not a discrete, capturable event as it would appear in an ideal simulator. The guard event for leg swapping is defined here in terms of step duration and measured vertical ground reaction force. In general, a gait timing variable is a strictly monotonically increasing quantity that varies from 0 to 1 over the course of a step. Here we use $\tau = \frac{t-t_0}{T_p}$, where t_0 is the starting time of the current step and T_p is the time duration of a step. The guard for leg swapping is then

$$(GRF_{swing}^z > GRF_{min} \text{ and } \tau > 0.5) \quad (6)$$

or $\tau > 1$,

14 where GRF_{swing}^z is the measured vertical component of the ground reaction force acting on the swing foot and GRF_{min} is a chosen minimum threshold.

16 PHZD: Control Policy Design on the Basis of a Single Periodic Gait

Given the hybrid model of the system as in (3), the first objective of this article is to design a feedback control policy that creates and robustly stabilizes a single periodic solution of the exoskeleton. Specifically, we view the combined fully actuated exoskeleton and its user as a 3D bipedal mechanism. In this section, a brief description of the well-studied virtual constraints-based feedback control law for a single periodic gait is presented. In a later section, a control methodology that addresses more complex dynamical behaviors of the exoskeleton is introduced.

Virtual Constraints

24 At the core of this method is the design of a set of virtual constraints that modulate the joint trajectories of the system in order to achieve certain desired behaviors [46], [59]. Enforcing **26** virtual constraints results in a lower dimensional representation of the full-order system—termed the partial hybrid zero dynamics (PHZD)—that captures the natural dynamics of the mechanical system. While the PHZD is a reduced-order model, it does not involve any approximations of **28** the dynamics. Solutions of the PHZD are solutions of the original system model under feedback control.

The virtual constraints are defined as the difference between actual physical quantities and their desired evolution, and then posed as outputs of the system that are to be zeroed by a feedback controller. In general, the actual outputs, y^a , represent important kinematic functions of the robot: they could be as simple as particular joint variables, such as the hip and knee angles, or they could also be more complicated functions of robot states, such as swing foot orientation in the world frame or forward velocity of the pelvis. The desired outputs are often represented by a group of parametrized curves with a timing variable. In their traditional form, the virtual constraints are synchronized through a state-based timing variable. Work in [60] and [61] show that such a state-dependent design is not strictly required. In order to present the main idea of a virtual-constraints-based feedback control design, a state-based phase variable is still assumed in this section.

For the particular case of the human-exoskeleton system with powered ankle joints, the actual outputs are chosen to be a combination of a velocity regulating term y_1^a and posture modulating terms y_2^a . Specifically, the velocity regulating output is the forward hip velocity of the exoskeleton, and posture modulating outputs are chosen to represent the synchronized motion of the remaining actuated joints. Hence, the virtual constraints for the exoskeleton are defined as

$$y_1(q, \dot{q}, \alpha) = y_1^a(q, \dot{q}) - y_1^d(\alpha), \quad (7)$$

$$y_2(q, \alpha) = y_2^a(q) - y_2^d(\theta(t), \alpha), \quad (8)$$

where y_1 and y_2 are relative degree 1 and (vector) relative degree 2 by construction, and θ is a “phasing variable” [62]. To fully determine a motion of the entire system, the outputs, (y_1^a, y_2^a) , must be linearly independent and their rank must be equal to the number of actuators in the system. y_1^a is set to be the forward hip velocity, while y_2^a is set to be the all joint angles of the exoskeleton except for the sagittal stance ankle [54].

Input Output Linearization.

With the goal of driving the virtual constraints in (7) and (8) to zero exponentially, the following feedback control law, based on Input Output Linearization, is considered,

$$u = -\mathcal{A}^{-1} \left(\begin{bmatrix} L_f y_1(q, \dot{q}, \alpha) \\ L_f^2 y_2(q, \dot{q}, \alpha) \end{bmatrix} + \begin{bmatrix} \epsilon y_1(q, \dot{q}, \alpha) \\ 2\epsilon \dot{y}_2(q, \dot{q}, \alpha) \end{bmatrix} + \begin{bmatrix} 0 \\ \epsilon^2 y_2(q, \alpha) \end{bmatrix} \right), \quad (9)$$

with a control gain $\epsilon > 0$ and *decoupling matrix*

$$\mathcal{A} = \begin{bmatrix} L_g y_1^a(q, \dot{q}) \\ L_g L_f y_2(q, \dot{q}, \alpha) \end{bmatrix}, \quad (10)$$

where L_f and L_g represents the Lie derivatives with respect to the vector fields $f(x)$ and $g(x)$ in (3). With a specific choice of virtual constraints, the decoupling matrix \mathcal{A} is invertible. Applying this control law to (3) yields linear output dynamics of the form:

$$\dot{y}_1 = -\frac{1}{\epsilon}y_1, \quad (11)$$

$$\ddot{y}_2 = -2\frac{1}{\epsilon}\dot{y}_2 - \frac{1}{\epsilon^2}y_2, \quad (12)$$

which has an exponentially stable equilibrium at the origin.

2 Hence, the directly actuated variables of the system are regulated to a reduced-dimensional
 4 surface called the *zero dynamics* that is invariant within the duration of continuous swing phase,
 6 as illustrated in Figure 5a [46], [59]. Yet, due to the discrete joint velocity changes in the
 8 system's states at swing foot impact, the controller in (9) does not necessarily guarantee the
 10 reduced-dimensional surface is invariant through the impact. It is shown in [46] that, if there
 12 exists a set of virtual constraints such that the reduced-dimensional zero dynamics surface is
 14 invariant through impact, then the full-order dynamics of the hybrid system model restricts
 to a *hybrid-invariant* reduced-dimensional submanifold. The restriction dynamics and invariant
 surface is the *hybrid zero dynamics* (HZD). This requires one to find a set of parameters α
 for the virtual constraints such that the zero dynamics is invariant through impact maps (see
 Figure 5b). Finding such parameters is typically formulated as a nonlinear optimization problem
 [50], [59]. The advantage of studying the hybrid zero dynamics manifold is that the evaluation
 of orbital stability of the full-order system can be performed on the reduced-dimensional zero
 dynamics.

16 Generation of a Periodic Gait

Periodic walking gaits are periodic orbits of the corresponding hybrid system model. A
 18 solution $\varphi(t)$ of the hybrid system in (3) is *periodic* if there exist a finite $T > 0$ such that
 20 $\varphi(t + T) = \varphi(t)$ for all $t \in [t_0, \infty)$. A set $\mathcal{O} \subset T\mathcal{Q}$ is a periodic orbit of the system if
 22 $\mathcal{O} = \{\varphi(t) | t \geq t_0\}$ for some periodic solution $\varphi(t)$. The stability of the periodic orbit can be
 determined by the stability of the fixed point by evaluating the spectral radius of the Jacobian
 of the Poincaré map at the fixed point. More specifically, if all eigenvalues lie within the unit
 circle, i.e., have magnitude less than 1, then the periodic orbit is locally exponentially stable.

24 To design a periodic gait for the hybrid system model of the exoskeleton, a direct
 26 collocation-based gait optimizer is used. The mathematical foundation behind the optimization
 technique used is briefly introduced in the sidebar “How Direct Collocation Works”. Other ways
 28 of solving the optimization can be used, such as single shooting methods, but direct collocation
 was found to be the fastest and most efficient way to solve this problem [50]; stable walking

gaits are obtained in minutes. Considering that our goal in this section is to find parameters for
2 the virtual constraints instead of open-loop trajectories, we incorporate the feedback controller
into the optimization in a way that is similar to holonomic constraints. Instead of enforcing the
4 control input directly as in (9), we impose equality constraints on system states such that they
satisfy the output dynamics in (11) and (12). Furthermore, the hybrid-invariance is enforced in
6 the periodic gait optimization as a constraint. For a detailed setup of the optimization problem in
the context of the exoskeleton, the reader is referred to [53], [54]. Torque limits and joint position
8 and velocity limits of the ATALANTE mechanism are directly enforced as boundary conditions
on decision variables in the optimization, whereas friction cone and zero moment constraints
10 of foot contacts are enforced as extra physical constraints. In addition, several constraints are
considered in the optimization in order to narrow down the search space and address certain
12 aspects specific to human-friendly walking. Impact velocities, ZMP position, CoM position and
torso orientation are examples of the many constraints that need to be considered.

14 The result of the optimization is a single periodic orbit and a feedback controller that
renders it locally exponentially stable in the model of the user plus exoskeleton. Simulations of
16 the controller can be found in [53] and are not given here. The experiments reported later are
based on the design process described above.

18 GHZD-Harnessing the Power of Modern Optimization Techniques

When the HZD and PHZD methods were created, it would take several hours for the
20 computation of a single periodic orbit. At that time, it was very important to be able to build
a controller for rendering the periodic orbit locally exponentially stable directly from the orbit
22 itself, without requiring further optimizations. The situation today is totally different as shown
in Table 1. So, how to harness this power?

24 The control loops on the exoskeleton run at 1 KHz and the duration of a walking step is on
the order of 500 ms to 750 ms. Hence, online Model Predictive Control (MPC) (i.e., iteratively
26 solving in real time a finite-horizon constrained optimization problem) is simply not possible
for models with twenty or more state variables. Explicit MPC is not possible either because one
28 would have to numerically sample the state space, do the optimization offline, and then store
the control actions for use online. A sparse uniform grid of ten samples per dimension would
30 require 10^{20} optimizations; random sampling will provide a smaller, more effective discretization
of the state space, but not enough is gained to handle $n \geq 20$. So, what to do?

32 Reference [63] introduces GHZD, Generalized Hybrid Zero Dynamics, a new approach
to control design for a class of high-dimensional nonlinear systems. As with PHZD, the design

process for GHZD begins with trajectory optimization to design an open-loop periodic walking motion of the high-dimensional model. It differs from PHZD in that it exploits the fact the trajectory optimization can be done rapidly to add to this periodic solution a carefully selected set of additional open-loop trajectories of the model that steer toward the nominal motion, thereby directly building in stability. A drawback of trajectories is that they provide little information on how to respond to a disturbance. To address this shortcoming, Supervised Machine Learning is used to extract a low-dimensional state-variable realization of the open-loop trajectories. The periodic orbit is now an attractor of the low-dimensional state-variable model but is not attractive in the full-order system. The special structure of mechanical models associated with bipedal robots is used to embed the low-dimensional model in the original model in such a manner that the desired walking motions are locally exponentially stable.

In the following, we give the main ideas underlying GHZD for models given by ordinary differential equations; the reader is referred to [63] for the small technical changes required to deal with hybrid models.

Step 1: Constructing Z_0 , the boundary of the generalized HZD surface, from a collection of periodic orbits.

The [dynamic](#) model of the exoskeleton is decomposed into a low-dimensional weakly actuated portion corresponding roughly to the $x - y$ -coordinates and velocities of the hips ([in the world frame](#)) and a strongly actuated portion of the model that captures the hips, knees, and swing ankle joints. Specifically, the [dynamic](#) portion of the hybrid model (3) is decomposed as

$$\begin{aligned}\dot{x}_1 &= f_1(x_1, x_2, u_1) \quad x_1 \in \mathbb{R}^{n_1} \\ \dot{x}_2 &= f_2(x_1, x_2, u_1, u_2) \quad x_2 \in \mathbb{R}^{n_2},\end{aligned}\tag{13}$$

where x_1 represents the “weakly actuated” portion of the model, u_1 are the stance ankle torques, x_2 captures the strongly actuated part of the model and the remaining actuators u_2 . With this decomposition, $n_1 \ll n_2$; indeed, for the exoskeleton as modeled here in single support, $n_1 = 4$ and $n_2 = 20$.

Next, a library of gaits is constructed by uniformly discretizing a bounded set of initial conditions for x_1 . Without loss of generality, each periodic gait is assumed to start from the origin, i.e., hip positions $(x; y)$ are at the origin. As a consequence, the periodic gaits are parametrized by the $(x; y)$ -velocities of the hip, corresponding to walking forwards, backwards, and sideways. Turning is not addressed presently but will be in the near future.

A nonlinear mapping is then constructed between the x_1 and x_2 states for the periodic orbits such that $x_2 = \gamma(x_1)$. The function γ is called an insertion map and can be constructed

in several ways. One effective approach is to numerically fit a surface to the initial conditions
₂ of the periodic orbits through machine learning tools, resulting in

$$Z_0 := \{x =: (x_1; x_2) | x_2 = \gamma(x_1)\}, \quad (14)$$

as illustrated in Figure 6. In the ideal case, every point on the surface Z_0 corresponds to an
₄ initial condition for a periodic orbit.

Step 2: Constructing Z , the Generalized HZD Surface.

Assume now that one of the periodic orbits has been selected, corresponding to a point
₆ on $\xi^* \in Z_0$. The process of stabilizing this particular periodic orbit is based on computing
₈ a judiciously selected set of open-loop trajectories of the full-order model that “approach” the
₁₀ periodic solution. Specifically, let B be an open ball about ξ^* and select a “contraction factor” $0 \leq$
₁₂ $c < 1$. For each initial condition $\xi \in B \cap Z_0$, a solution of the ODE (13) with initial condition ξ is
₁₄ sought that satisfies the physical constraints given in Section Gait Design Objectives, terminates
₁₆ in Z_0 at time $t = T_p$, and approaches the periodic solution as measured by $\|\varphi_\xi(T_p) - \xi^*\| \leq$
₁₈ $c\|\xi - \xi^*\|$; transient solutions that approach periodic solutions are called transition gaits.

Denote the input and corresponding solution parametrized by the initial condition as

$$\begin{aligned} u_\xi : [0, T_p] &\rightarrow \mathbb{R}^m, \\ \varphi_\xi : [0, T_p] &\rightarrow \mathbb{R}^n. \end{aligned} \quad (15)$$

If all has gone well, the process has resulted in a smooth surface of dimension equal to the
₁₆ dimension of Z_0 plus one (due to time), as shown in Figure 6. As discussed in [63], such
₁₈ solutions may or may not exist and in principle could be very “ugly” functions of ξ (i.e., non-
smooth, etc.). We note that because for all $\xi \in Z_0$, $\varphi_\xi(T_p) \in Z_0$, trajectories that start in Z_0 can
be continued indefinitely.

Step 3: State-variable Realization of the Open-loop Trajectories Forming Z .

While the above process results in complete trajectories for the model, we do not directly
₂₂ use these for tracking because: (a) If the system starts on the surface Z , and a perturbation
occurs between $t = 0$ and $t = T_p$, it would attempt to converge back to the potentially-far-away
₂₄ original-trajectory $\varphi_{xi}(t)$ until $t = T_p$, only at which point would a trajectory-based controller
update the desired trajectory; and (b), if the system does not start on the surface, there is no
₂₆ obvious choice of a trajectory to follow.

We first address (a) by seeking a means to continuously update the desired evolution of the
₂₈ system so as to immediately respond to a perturbation. In fact, we will design a low-dimensional

differential equation that evolves on the surface and has the desired periodic orbit as its locally
₂ stable and attractive limit cycle. A solution to (b) will be given in Step 5.

Figure 7 motivates a condition for “automatically re-planning” so as to respond to a
₄ disturbance, namely

$$x(t) = \varphi_\xi(t) \implies u(t, x(t)) = u_\xi(t). \quad (16)$$

This is an implicit interpolation condition for specifying a control response at each point of the
₆ surface Z in Figure 6. As explained further in [63], a solution to (16) can be constructed if one
₈ can find two T_p -periodic functions, ν and μ , satisfying the following conditions on the trajectory
₈ data: for all $0 \leq t < T_p$

$$\begin{aligned} \nu(t, \pi_1 \circ \varphi_\xi(t)) &= \pi_2 \circ \varphi_\xi(t) \\ \mu(t, \pi_1 \circ \varphi_\xi(t)) &= u_\xi(t), \end{aligned} \quad (17)$$

where $\pi_i : \mathbb{R}^n \rightarrow \mathbb{R}^{n_i}$ are the canonical projections (i.e., $\pi_1(x_1, x_2) = x_1$ and $\pi_2(x_1, x_2) = x_2$).

Moreover, it can then be shown that (i) the trajectories of Figure 6 are solutions of the reduced-order model

$$\begin{aligned} \dot{x}_1 &= f_1(x_1, \nu(t, x_1), \mu_1(t, x_1)), \\ x_2 &= \nu(t, x_1), \end{aligned} \quad (18)$$

and that (ii) the periodic orbit $\varphi_{\xi^*} : [0, T_p] \rightarrow \mathbb{R}^n$ is locally exponentially stable. In fact, by construction, all initial conditions $\xi \in Z_0$ for which feasible model solutions have been found result in trajectories that converge to the periodic orbit; hence, as one builds the feasible solutions in (15), one is constructing the domain of attraction of the periodic orbit in the G-HZD surface,
₁₆ Z .

Figure 8 shows the sagittal-plane hip velocity for several initial conditions in Z_0 . Two things are important to note: (a) the convergence to the nominal orbit; and (b), the trajectories are feasible solutions of the full-order model.

Next we deal with how to find functions satisfying the conditions in (17).

Step 4: Supervised Machine Learning to Extract ν and μ from Optimization Data

The importance of finding a differential equation (i.e., vector field) realization of the trajectories in Figure 6 is that the differential equation is an automatic, instantaneous re-planner of the system’s evolution when it is perturbed off a nominal motion. Figure 9 shows such a realization. Solving for the functions in (17) is the key to constructing the vector field. Doing so analytically would be a challenge at best, and this is where Supervised Machine Learning comes into play. Table 2 shows a vanilla implementation where the *features* are selected as time and

the x_1 -states and the *labels or targets* are taken as the inputs u and the x_2 -states. In the control implementations simulated here, the features are taken as the Cartesian hip velocities only (the positions are discarded) and the labels are taken as the outputs listed in Table 3.

At this point we have all the functions we need to implement a control policy that locally exponentially stabilizes the selected periodic walking gait. Figure 10 shows one component of the function ν arising from the Supervised Machine Learning.

Step 5: Feedback Control to Render Z Attractive.

The previous steps created a low-dimensional dynamical model for which the desired periodic orbit with initial condition $\xi^* \in Z_0$ is locally stable and attractive in Z . The next step is to stabilize the orbit in the full model, as illustrated in Figure 11, and for this we need to be more specific about the x_2 -portion of the model. In the case of the exoskeleton, strongly actuated part of the model is fully actuated and is therefore feedback linearizable [64]. In particular, the x_2 -part of the model (13) can be expressed as

$$x_2 = \begin{bmatrix} x_{2a} \\ x_{2b} \end{bmatrix} \text{ and } f_2 = \begin{bmatrix} x_{2b} \\ \alpha(x_1, x_2) + \beta_1(x_1, x_2)u_1 + \beta_2(x_1, x_2)u_2 \end{bmatrix}, \quad (19)$$

where β_2 is square and invertible.

In [63], it is shown that for all $\frac{n_2}{2} \times \frac{n_2}{2}$ positive definite matrices K_p and K_d , $\varphi_{\xi^*} : [0, T_p] \rightarrow \mathbb{R}^{n_2}$ is a locally uniformly exponentially stable solution of the closed-loop system

$$\begin{aligned} \dot{x}_1 &= f_1(x_1, x_2, u_1) \\ \dot{x}_2 &= f_2(x_1, x_2, u_1, u_2) \\ u_1 &= v_1 \\ u_2 &= [\beta_2(x_1, x_2)]^{-1} (-\alpha(x_1, x_2) - \beta_1(x_1, x_2)u_1 + v_2) \\ \begin{bmatrix} v_1 \\ v_2 \end{bmatrix} &= \mu(t, x_1) - [K_p \ K_d](x_2 - \nu(t, x_1)). \end{aligned} \quad (20)$$

Step 6 (Optional): Enriching the Control Policy to Handle Multiple Gaits

The final step performed with the ATALANTE model is to repeat the above processes for a grid of periodic gaits corresponding to a range of walking speeds captured in Z_0 . The trajectory designs for these new gaits are catenated to Table 2, with the only change being that the feature set is augmented to include the designed average (Cartesian) velocity of each gait. Supervised Machine Learning, if successful, then produces a control policy that allows a desired walking speed to be selected.

Remark on Trajectory Design via Optimization

We provide a few details on how to actually generate the trajectories in (15) that form the surface in Figure 6. We use optimization to determine solutions of the model; see “How Direct Collocation Works” for more details on the optimization method itself. In particular, a cost function of the form

$$\begin{aligned} J(\xi) = \min_{u_\xi} & \int_0^{3T_p} L(\varphi_\xi(\tau), u_\xi(\tau)) d\tau \\ \text{s.t. } & \varphi_\xi(t) = \xi + \int_0^t f(\varphi_\xi(\tau), u_\xi(\tau)) d\tau \\ & 0 \geq c(\varphi_\xi(t), u_\xi(t)), \quad 0 \leq t \leq 3T_p \\ & \varphi_\xi(T_p) \in Z_0, \quad \|\varphi_\xi(T_p) - \xi^*\| \leq c\|\xi - \xi^*\| \\ & \varphi_\xi(3T_p) = \xi^* \end{aligned} \tag{21}$$

with constraints is posed over a time horizon of three steps such that (i) energy per step taken is penalized, (ii) solutions satisfy the full-order model, (iii) key constraints on ground reaction forces and actuator limits are respected (captured in the function $c \leq 0$), (iv) solution returns to Z_0 in one step so that trajectories can be continued indefinitely, while approaching the desired periodic orbit, and (v) terminates at the nominal periodic orbit in three steps (this could be replaced by a terminal penalty in the cost function). The choice of three (robot) steps in the optimization is based on the capture-point analysis in [65] and theoretical work in [63]. $L(\varphi_\xi(\tau), u_\xi(\tau))$ defines the running cost while $f(\varphi_\xi(\tau), u_\xi(\tau))$ is the dynamics of the system. Figure 12 shows a conceptual representation of the gait design process.

Numerical Illustration

This section presents simulation results of the GHZD-controller developed in the previous section. The simulation experiments were done with Gazebo using the full dynamical model of the exoskeleton with a human in it. The ground contact model in Gazebo allows the possibility for the feet to roll and slip. In these tests, the machine learning was used to stabilize forward walking by looking at gaits for different forward and backward walking speeds in the range of -0.3 m/s to 0.3 m/s.

Velocity Tracking

Figure 13 shows a simulation where the exoskeleton starts with stepping in-place at $t = 0$ s, then at $t = 3$ s, the exoskeleton is commanded to walk at a speed of 0.15 m/s, until at $t = 10$ s, the exoskeleton is commanded to return to a stepping in place gait. It can be seen that there

is a small steady-state error when forward walking is commanded; this can be attributed to a
2 combination of joint tracking errors from the low-level PD-controllers and the compliant (non-
rigid) ground being different from the model used for control design. Figure 14 shows the gait
4 timing variable exhibiting a typical triangle-wave pattern, with leg swapping happening before
 $\tau = 1$. It can be seen that regardless of whether the system was in a periodic gait or was
6 transitioning between speeds, τ consistently terminates at around 0.9. This is due to having
8 trained the system on various transition gaits. The phase portrait given in Figure 15 shows
the periodic nature of stepping in-place, followed by a transient to another periodic condition.
Convergence to periodic motion is clear during periods when the speed command is constant.
10 Stick figures showing step-in-place, transitioning, and walking forward can be seen in Figure 16.
An animated video of the simulation result can be seen in [66].

12 Force Perturbation Rejection

In this test, we apply external perturbation forces of different magnitudes and directions
14 to the exoskeleton while walking. We compare the response of two different configurations:
one with the controller using the Supervised Machine Learning and another with a fixed single
16 periodic gait. The external force is applied at the hip of the exoskeleton during the second step
for 0.1 s in either forward or backward directions. The exoskeleton is commanded to walk in
18 place throughout the test. The Gazebo simulation results are shown in Figure 17 and Figure 18.
In particular, using Supervised Machine Learning, the exoskeleton was able to recover from up
20 to 750 N force in the forward direction and 650 N force in the backwards direction, whereas
the system lost stability with any forward force larger than 300 N and backward force larger
22 than 100 N when using the fixed periodic gait profile. Figure 17 shows the changes in the
forward hip velocity of the exoskeleton for both Supervised Machine Learning and fixed gaits
24 method. It is shown that the Supervised Machine Learning controller is capable of recovering
for very large velocity disturbances due to the external forces. In addition, Figure 18 shows how
26 the controllers respond to the external disturbances by changing the desired trajectories of the
exoskeleton joints. Specifically, the Supervised Machine Learning controller extending the swing
28 leg outward with respect to large perturbation by changing the desired trajectory of the sagittal
swing hip joint. This behavior occurs naturally from training using optimized walking gaits for
30 different speeds and transitions among them. The fixed gait controller solely uses the large feet
of the exoskeleton to reject the perturbation instead of adjusting the desired trajectories. An
32 animated video of the force perturbation simulations in Gazebo can be seen in [66].

Preliminary Experimental Results using PHZD

2 Experimental implementation of the biped-inspired control laws has begun, with very
3 promising results as alluded to in the opening lines of this article. Because the PHZD control laws
4 have been extensively evaluated on several bipedal robot platforms, they have been employed
5 in the initial testing. The results described here are under review for publication in [54]. The
6 reviewers are asked to be especially careful about not sharing the video [67] with colleagues.

8 In the first evaluation of the controllers, a mannequin or dummy was placed in the
9 exoskeleton as shown in Figure 19. As we can see in Figure 20, the nominal and target trajectories
10 ([in red and blue respectively](#)) are marginally different after the tuning and high-level filtering of
11 the nominal trajectories. The target gait is followed with relatively good accuracy resulting in
12 stable dynamic walking of the hardware.

12 Experimental results with human subjects

14 As a result of the successful results obtained with the mannequin, experiments are carried
15 out with paraplegic patients. [All patients are complete paraplegic, unable to stand by themselves,](#)
16 [unable to walk, with lesion ranged from T12 to T6.](#) Some characteristics of these patients are
17 summarized in Table 4.

18 Experiments were conducted in a certified medical center and approved by the ANSM
19 (French regulatory administration for health products). To prevent injury from a fall, one person
20 is placed at each side of a patient. In case of loss of balance, the two assistants catch the
21 exoskeleton by handles on its sides. Furthermore, a safety cable is attached to the exoskeleton
22 and an overhead rail (or gantry). This is a secondary means to secure a patient and prevent a
23 fall. To be clear, assistance is provided only in case of loss of balance. During walking, the
24 exoskeleton and its user are self-stabilized and no outside assistance was given.

25 As can be seen in the video at [67] and Figure 21, crutch-less dynamically stable
26 exoskeleton walking of paraplegic patients is achieved as a result of the methodology developed
27 for bipedal robots. All patients managed to walk unassisted for the entire length of the room
28 after a few trials during which a best gait was chosen and then tuned; Table 4 includes the speed
29 of walking and distance traveled.

30 The ability to successfully transfer the formal gaits generated to hardware is illustrated
31 in Figure 22 for Patient A, wherein the nominal (blue) and measured (shaded) trajectories are
32 consistent throughout the experiment. [The tracking error at the joint level for Patient A can](#)
33 [be seen in Figure 23.](#) The motor torques resulting from tracking the nominal trajectories (cf.

Figure 24) are also consistent with simulation. Note that motor-torque saturations are relatively uncommon as the gaits are designed to account for all hardware limits. To compare the walking between patients, a representative selection of phase portraits for each patient are presented in Figure 25; even though the gaits are not the same (as they have been generated to best suit each patient), they all display a common fundamental structure. This is further illustrated in gait tiles of the patients walking in the exoskeleton (cf. Figure 21).

Next steps

While the dynamic walking gaits obtained are preliminary, and in no way constitute any kind of clinical evaluation, the ability to consistently realize them on patients points toward the validity of the framework being pursued. During the preliminary testing, the few tests that failed to completely traverse the lab were caused by foot scuffing or loss of lateral balance. In the next phase of testing, we will evaluate the GHZD controllers discussed in the previous two sections.

Future Work

While this paper presents an important accomplishment, a lot remains to be done in the field of actively controlled exoskeletons. Future research directions involve developing control algorithms that (a) directly address model uncertainty; (b) support a rich set of behaviors such as standing and sitting and dynamic transitions between these; (c) enable push recovery and robustness to significant force disturbances that could arise due to contact with the environment or other humans; (d) use models of human comfort so as to balance between comfort and robustness of a gait of the exoskeleton; (e) capture human intent so as to enable human-driven autonomous exoskeleton control; (f) adapt to and provide user customized behaviors; and (g) improve the energy efficiency of assisted walking. **Regarding model uncertainty, it is hoped that methods developed in [68] can be incorporated into the optimization and machine learning methods to provide robust nominal orbits.**

We believe methods presented in this paper can be extended to tackle many of these tasks. For example, Figure 26 shows preliminary results for a transition from sitting to standing obtained via optimization. In the model, it was assumed that the user can use their arms to assist liftoff by applying an external force on the chair up to half their body weight. It can be seen from Figure 27 that most of the force is used to push the user horizontally off the chair.

Conclusions

2 The ATALANTE exoskeleton studied in this paper is the first to allow dynamic hands-
3 free walking for paraplegics. Where other devices require crutches for lateral stabilization, the
4 embedded control algorithms on the studied exoskeleton regulate leg motion so as to sustain
5 a locally exponentially stable walking gait. The keys to realizing crutch-less dynamic walking
6 were novel hardware, stiff enough to physically support a subject, powerful enough to move the
7 device's legs quickly, and novel control mathematics developed over the past 15 years to allow
8 bipedal robots to walk stably in uncertain environments and with imprecise dynamic models.

10 The preliminary experimental results have demonstrated very slow walking on the order
11 of 0.1 m/s. Stable gaits at 0.4 m/s have been achieved in simulation, and such speeds can be
12 expected to be reached on the current hardware and with patients. New tools are coming online
13 for the rapid computation of trajectories for high-degree-of-freedom mechanical systems as well
14 as new control methods that are providing ways to mitigate the curse of dimensionality. A path
forward to restoring locomotion for paraplegics is becoming more and more clear.

Acknowledgments

2 The US investigators are covered under IRB protocol number 16-0693. The French
investigators are covered under CPP Ile de France XI, number 16041.

4 The authors thank the entire Wandercraft team who designed ATALANTE as well as
implemented and tested the control algorithms used in the experiments. Additionally, the
6 authors are grateful to Laurent Praly and Nicolas Petit, researchers at CAS (Mines ParisTech,
PSL Research University) for their scientific support since the founding of Wandercraft. The
8 authors thanks Xingye (Dennis) Da for his consultation on GHZD.

10 The work of A. Hereid was supported by NSF under Grant CPS-1239037. The work of O.
Harib and J. W. Grizzle was supported in part by NSF Grant NRI-1525006 and in part by a gift
12 from Ford Motor Company. M.E. Mungai is supported by a University of Michigan Fellowship.
The work of A. Agrawal and K. Sreenath is supported by NSF grant IIS-1526515. The work of
14 Thomas Gurriet and Aaron Ames was supported by NSF NRI award 1526519.

References

- [1] “Wandercraft,” <http://www.wandercraft.eu/en/>—, note=Accessed: 2017-11-07, Nov 2017.
- [2] A. M. Dollar and H. Herr, “Lower extremity exoskeletons and active orthoses: Challenges and state-of-the-art,” *IEEE Trans. Robot.*, vol. 24, no. 1, pp. 144–158, 2008.
- [3] K. Ziegler-Graham, E. J. MacKenzie, P. L. Ephraim, T. G. Travison, and R. Brookmeyer, “Estimating the prevalence of limb loss in the united states: 2005 to 2050,” *Arch. Phys. Med. Rehab.*, vol. 89, no. 3, pp. 422–429, 2008.
- [4] R. L. Waters, J. Perry, D. Antonelli, and H. Hislop, “Energy cost of walking of amputees: The influence of level of amputation,” *J. Bone Joint Surg. Amer.*, vol. 58, no. 1, pp. 42–46, January 1976.
- [5] J. P. Pell, P. T. Donnan, F. G. Fowkes, and C. V. Ruckley, “Quality of life following lower limb amputation for peripheral arterial disease,” *Eur. J. Vasc. Surg.*, vol. 7, no. 4, pp. 448–451, 1993.
- [6] W. Miller, A. Deathe, M. Speechley, and J. Koval, “The influence of falling, fear of falling, and balance confidence on prosthetic mobility and social activity among individuals with a lower extremity amputation,” *Arch. Phys. Med. Rehab.*, vol. 82, no. 9, pp. 1238–1244, 2001.
- [7] H. I. Krebs, N. Hogan, M. L. Aisen, and B. T. Volpe, “Robot-aided neurorehabilitation,” *IEEE transactions on rehabilitation engineering*, vol. 6, no. 1, pp. 75–87, 1998.
- [8] P. R. Geigle and M. Kallins, “Exoskeleton-assisted walking for people with spinal cord injury,” *Archives of Physical Medicine and Rehabilitation*, vol. 98, no. 7, pp. 1493–1495, 2017.
- [9] A. M. Dollar and H. Herr, “Lower Extremity Exoskeletons and Active Orthoses:Challenges and State-of-the-Art,” *IEEE Transactions on Robotics*, vol. 24, no. 1, pp. 144–158, 2008.
- [10] A. J. Young and D. P. Ferris, “State of the Art and Future Directions for Lower Limb Robotic Exoskeletons.” *IEEE transactions on neural systems and rehabilitation engineering : a publication of the IEEE Engineering in Medicine and Biology Society*, vol. 25, no. 2, pp. 171–182, 2017.
- [11] W. Huo, S. Mohammed, J. C. Moreno, and Y. Amirat, “Lower Limb Wearable Robots for Assistance and Rehabilitation: A State of the Art,” *IEEE Systems Journal*, vol. 10, no. 3, pp. 1068–1081, 2016.
- [12] R. S. Mosher, “Handyman to hardiman,” SAE Technical Paper, Tech. Rep., 1967.
- [13] J. Grundmann and A. Seireg, “Computer control of multi-task exoskeleton for paraplegics,” *Proceedings of the Second CISIM/IFTOMM International Symposium on the Theory and Practice of Robots and Manipulators*, pp. 233–240, 1977.
- [14] M. Vukobratovic, D. Hristic, and Z. Stojiljkovic, “Development of active anthropomorphic

- exoskeletons," *Medical and Biological Engineering*, vol. 12, no. 1, pp. 66–80, 1974.
- [15] D. Hristic, M. Vukobratovic, and M. Timotijevic, "New model of autonomous' active suit'for dystrophic patients," in *Proceedings of the International Symposium on External Control of Human Extremities*, 1981, pp. 33–42.
- [16] "Ekso Bionics," <http://eksobionics.com/>, accessed: 2017-11-04.
- [17] "ReWalk 6.0 - Home," <http://rewalk.com/>, accessed: 2017-11-04.
- [18] G. Zeilig, H. Weingarden, M. Zwecker, I. Dudkiewicz, A. Bloch, and A. Esquenazi, "Safety and tolerance of the ReWalk exoskeleton suit for ambulation by people with complete spinal cord injury: A pilot study," *The Journal of Spinal Cord Medicine*, vol. 35, no. 2, pp. 96–101, 2012. [Online]. Available: <http://www.tandfonline.com/doi/full/10.1179/2045772312Y.0000000003>
- [19] K. Suzuki, G. Mito, H. Kawamoto, Y. Hasegawa, and Y. Sankai, "Intention-Based Walking Support for Paraplegia Patients with Robot Suit HAL," *Advanced Robotics*, vol. 21, no. 12, pp. 1441–1469, 2007. [Online]. Available: <http://www.tandfonline.com/doi/abs/10.1163/156855307781746061>
- [20] "HAL for medical use (Lower Limb Type)," https://www.cyberdyne.jp/english/products/LowerLimb_medical.html—, note=Accessed: 2017-11-06, Nov 2017.
- [21] R. Jimenez-Fabian and O. Verlinden, "Review of control algorithms for robotic ankle systems in lower-limb orthoses, prostheses, and exoskeletons," *Med. Eng. Phys.*, vol. 34, no. 4, pp. 397–408, 2012.
- [22] F. Sup, A. Bohara, and M. Goldfarb, "Design and control of a powered transfemoral prosthesis," *The International journal of robotics research*, vol. 27, no. 2, pp. 263–273, 2008.
- [23] A. Simon, N. Fey, S. Finucane, R. Lipschutz, and L. Hargrove, "Strategies to reduce the configuration time for a powered knee and ankle prosthesis across multiple ambulation modes," in *IEEE Int. Conf. Rehab. Robot.*, Seattle, WA, 2013.
- [24] A. M. Simon, K. A. Ingraham, N. P. Fey, S. B. Finucane, R. D. Lipschutz, A. J. Young, and L. J. Hargrove, "Configuring a powered knee and ankle prosthesis for transfemoral amputees within five specific ambulation modes," *PloS one*, vol. 9, no. 6, p. e99387, 2014.
- [25] R. D. Gregg, T. Lenzi, L. J. Hargrove, and J. W. Sensinger, "Virtual constraint control of a powered prosthetic leg: From simulation to experiments with transfemoral amputees," *IEEE Transactions on Robotics*, vol. 30, no. 6, pp. 1455–1471, October 2014.
- [26] E. Stickland, "Good-bye, wheelchair," *IEEE Spectrum*, vol. 49, no. 1, pp. 30–32, January 2012.
- [27] R. Angold, N. Harding, and H. Kazerooni, "Semi-powered lower extremity exoskeleton," Nov. 15 2011, uS Patent 8,057,410. [Online]. Available: <https://www.google.com/patents/US8057410>

- [28] K. Anam and A. A. Al-Jumaily, “Active exoskeleton control systems: State of the art,” *Journal of Procedia Engineering*, vol. 41, pp. 988–994, 2012.
- [29] M. R. Tucker, J. Olivier, A. Pagel, H. Bleuler, M. Bouri, O. Lambercy, J. d. R. Millán, R. Riener, H. Vallery, and R. Gassert, “Control strategies for active lower extremity prosthetics and orthotics: a review,” *Journal of NeuroEngineering and Rehabilitation*, vol. 12, no. 1, p. 1, Jan 2015. [Online]. Available: <https://doi.org/10.1186/1743-0003-12-1>
- [30] G. Suzuki, K., H. Mito, Y. Kawamoto, Hasegawa, and Y. Sankai, “Intention-based walking support for paraplegia patients with robot suit hal,” *Advanced Robotics*, vol. 21, no. 12, pp. 1441–1469, 2007.
- [31] G. Aguirre-Ollinger, J. Colgate, M. Peshkin, and A. Goswami, “Active-impedance control of a lower-limb assistive exoskeleton,” in *IEEE International Conference on Rehabilitation Robotics*, 2007.
- [32] M. Gomes, G. Silveira, and A. Siqueira, “Gait pattern adaptation for an active lower-limb orthosis based on neural networks,” *Advanced Robotics*, vol. 25, no. 15, pp. 1903–1925, 2011.
- [33] T. Nef, M. Guidali, and R. Riener, “Armin iiiarm therapy exoskeleton with an ergonomic shoulder actuation,” *Applied Bionics and Biomechanics*, vol. 6, no. 2, pp. 127–142, 2009.
- [34] A. Frisoli, E. Sotgiu, C. Procopio, M. Bergamasco, B. Rossi, and C. Chisari, “Design and implementation of a training strategy in chronic stroke with an arm robotic exoskeleton,” in *IEEE International Conference on Rehabilitation Robotics*, 2011.
- [35] S. Jezernik, G. Colombo, T. Keller, H. Frueh, and M. Morari, “Robotic orthosis lokomat: a rehabilitation and research tool,” *Neuromodulation: Technology at the Neural Interface*, vol. 6, no. 2, pp. 108–115, 2003.
- [36] A. Tsukahara, Y. Hasegawa, and Y. Sankai, “Gait support for complete spinal cord injury patient by synchronized leg-swing with hal,” in *IEEE/RSJ International Conference on Intelligent Robots and Systems*, 2011.
- [37] O. Unluhisarcikli, M. Pietrusinski, B. Weinberg, P. Bonato, and C. Mavroidis, “Design and control of a robotic lower extremity exoskeleton for gait rehabilitation,” in *IEEE/RSJ International Conference on Intelligent Robots and Systems*, 2011.
- [38] E. Wolbrecht, D. Reinkensmeyer, and J. Bobrow, “Pneumatic control of robots for rehabilitation,” *The International Journal of Robotics Research*, vol. 29, no. 1, pp. 23–38, 2010.
- [39] E. Rocon, J. Belda-Lois, A. Ruiz, M. Manto, J. Moreno, and J. Pons, “Design and validation of a rehabilitation robotic exoskeleton for tremor assessment and suppression,” *IEEE Transactions on Neural Systems and Rehabilitation Engineering*, vol. 15, no. 3, pp. 367–378, 2007.
- [40] K. Sreenath, H. Park, I. Poulikakos, and J. W. Grizzle, “Embedding active force control

- within the compliant hybrid zero dynamics to achieve stable, fast running on MABEL,”
 2 *International Journal of Robotics Research*, vol. 32, no. 3, pp. 324–345, 2013. [Online].
 Available: <https://doi.org/10.1177/0278364912473344>
- [41] S. Feng, E. Whitman, X. Xinjilefu, and C. G. Atkeson, “Optimization-based full body control for the DARPA Robotics Challenge,” *Journal of Field Robotics*, vol. 32, no. 2, pp. 293–312, 2015.
- [42] S. Kuindersma, F. Permenter, and R. Tedrake, “An efficiently solvable quadratic program for stabilizing dynamic locomotion,” in *Robotics and Automation (ICRA), 2014 IEEE International Conference on*. IEEE, 2014, pp. 2589–2594.
- [43] H. Dai, A. Valenzuela, and R. Tedrake, “Whole-body motion planning with centroidal dynamics and full kinematics,” in *2014 14th IEEE-RAS International Conference on Humanoid Robots (Humanoids)*. IEEE, 2014, pp. 295–302.
- [44] T. Koolen, J. Smith, G. Thomas, S. Bertrand, J. Carff, N. Mertins, D. Stephen, P. Abeles, J. Englsberger, S. Mccrory *et al.*, “Summary of team ihm’s virtual robotics challenge entry,” in *Humanoid Robots (Humanoids), 2013 13th IEEE-RAS International Conference on*. IEEE, 2013, pp. 307–314.
- [45] R. Tedrake, M. F. Fallon, S. Karumanchi, S. Kuindersma, M. E. Antone, T. Schneider, T. M. Howard, M. R. Walter, H. Dai, R. Deits *et al.*, “A summary of team mit’s approach to the virtual robotics challenge.” in *ICRA*, 2014, p. 2087.
- [46] E. R. Westervelt, J. W. Grizzle, C. Chevallereau, J. H. Choi, and B. Morris, *Feedback control of dynamic bipedal robot locomotion*. CRC press Boca Raton, 2007.
- [47] B. Griffin and J. Grizzle, “Walking gait optimization for accommodation of unknown terrain height variations,” in *2015 American Control Conference*, 2015, pp. 4810–4817.
- [48] K. Galloway, K. Sreenath, A. D. Ames, and J. W. Grizzle, “Torque saturation in bipedal robotic walking through control lyapunov function based quadratic programs,” *IEEE Access*, vol. 3, pp. 323–332, Apr. 2015.
- [49] Q. Nguyen and K. Sreenath, “Optimal robust control for bipedal robots through control lyapunov function based quadratic programs,” in *Robotics: Science and Systems*, Rome, Italy, 2015.
- [50] A. Hereid, E. A. Cousineau, C. M. Hubicki, and A. D. Ames, “3D dynamic walking with underactuated humanoid robots: A direct collocation framework for optimizing hybrid zero dynamics,” in *Robotics and Automation (ICRA), 2016 IEEE International Conference on*. IEEE, 2016, pp. 1447–1454.
- [51] D. Quintero, D. J. Villarreal, D. J. Lambert, S. Kapp, and R. D. Gregg, “Continuous-phase control of a powered knee-ankle prosthesis: Amputee experiments across speeds and inclines,” *To appear in IEEE Transactions on Robotics*, 2018.
- [52] H. Zhao, J. Horn, J. Reher, V. Paredes, and A. D. Ames, “Multicontact locomotion on

- transfemoral prostheses via hybrid system models and optimization-based control," *IEEE Transactions on Automation Science and Engineering*, vol. 13, no. 2, pp. 502–513, April 2016.
- [53] A. Agrawal, O. Harib, A. Hereid, S. Finet, M. Masselin, L. Praly, A. D. Ames, K. Sreenath, and J. W. Grizzle, "First steps towards translating HZD control of bipedal robots to decentralized control of exoskeletons," *IEEE Access*, vol. 5, pp. 9919–9934, 2017.
- [54] T. Gurriet, S. Finet, G. Boeris, A. Hereid, O. Harib, M. Masselin, J. Grizzle, and A. D. Ames, "Towards restoring locomotion for paraplegics: Realizing dynamically stable walking on exoskeletons," in *Submitted to 2018 IEEE International Conference on Robotics and Automation (ICRA)*. IEEE, 5 2018.
- [55] Y. Hurmuzlu, F. Génot, and B. Brogliato, "Modeling, stability and control of biped robots—a general framework," *Automatica*, vol. 40, no. 10, pp. 1647–1664, 2004.
- [56] J. W. Grizzle, C. Chevallereau, R. W. Sinnet, and A. D. Ames, "Models, feedback control, and open problems of 3D bipedal robotic walking," *Automatica*, vol. 50, no. 8, pp. 1955 – 1988, 2014. [Online]. Available: <http://www.sciencedirect.com/science/article/pii/S0005109814001654>
- [57] "urdf - ROS Wiki," <http://wiki.ros.org/urdf>, accessed: 2017-11-04.
- [58] A. Hereid and A. D. Ames, "Frost: Fast robot optimization and simulation toolkit," in *IEEE/RSJ International Conference on Intelligent Robots and Systems (IROS)*. Vancouver, BC, Canada: IEEE/RSJ, Sep 2017.
- [59] A. D. Ames, "Human-inspired control of bipedal walking robots," *IEEE Transactions on Automatic Control*, vol. 59, no. 5, pp. 1115–1130, 2014.
- [60] T. Wang and C. Chevallereau, "Stability analysis and time-varying walking control for an under-actuated planar biped robot," *Robot. Auton. Syst.*, vol. 59, no. 6, pp. 444–456, Jun. 2011. [Online]. Available: <http://dx.doi.org/10.1016/j.robot.2011.03.002>
- [61] J. Reher, E. A. Cousineau, A. Hereid, C. M. Hubicki, and A. D. Ames, "Realizing dynamic and efficient bipedal locomotion on the humanoid robot durus," in *Robotics and Automation (ICRA), 2016 IEEE International Conference on*. IEEE, 2016, pp. 1794–1801.
- [62] S. Kolathaya, J. Reher, and A. D. Ames, "Input to state stability of bipedal walking robots: Application to durus," *arXiv preprint arXiv:1801.00618*, 2018.
- [63] X. Da and J. Grizzle, "Combining Trajectory Optimization, Supervised Machine Learning, and Model Structure for Mitigating the Curse of Dimensionality in the Control of Bipedal Robots, submitted to the International Journal of Robotics Research," http://web.eecs.umich.edu/faculty/grizzle/papers/DaGrizzle_IJRR.pdf—, Nov 2017.
- [64] M. W. Spong, "Partial feedback linearization of underactuated mechanical systems," in *Intelligent Robots and Systems '94. 'Advanced Robotic Systems and the Real World', IROS*

- ² '94. *Proceedings of the IEEE/RSJ/GI International Conference on*, vol. 1, Sep 1994, pp. 314–321 vol.1.
- ⁴ [65] P. Zaytsev, S. J. Hasaneini, and A. Ruina, “Two steps is enough: No need to plan far ahead for walking balance,” in *2015 IEEE International Conference on Robotics and Automation (ICRA)*, May 2015, pp. 6295–6300.
- ⁶ [66] “Video of the gazebo simulation results.” https://youtu.be/7Ol-U1y_S8I.
- ⁸ [67] “Video of the experimental results.” <https://vimeo.com/233917538>, password: Atalante.
- ¹⁰ [68] B. Griffin and J. Grizzle, “Nonholonomic virtual constraints and gait optimization for robust walking control,” *The International Journal of Robotics Research*, vol. 36, no. 8, p. 0278364917708249, 2017.

TABLE 1: Performance comparison between direct-collocation optimization vs classic shooting approaches on a 5-link planar biped (single-shooting) and a 7-link spring-leg planar biped, respectively.

Method	CPU time (s)
Single shooting (<code>fmincon</code>)	162.59
Direct collocation (<code>IPOPT</code>)	1.60
Method	CPU time (s)
Multiple shooting (<code>fmincon</code>)	5027.45
Direct collocation (<code>IPOPT</code>)	41.47

TABLE 2: Conceptual arrangement of the optimization data from which appropriate functions for building a stabilizing controller can be determined by “regression”. Here ξ^i , $1 \leq i \leq M$ is a discretization of Z_0 , t_j , $1 \leq j \leq N$ is a discretization of $[0, T_p]$, $\varphi_{\xi}(t)$ is the solution of the full model with the initial condition ξ at $t = 0$, π_1 is the projection onto the x_1 coordinate, π_2 is the projection onto the x_2 coordinates, and $u_{\xi}(t)$ is the input giving rise to the solution $\varphi_{\xi}(t)$. Standard toolboxes in MATLAB are used to build the functions and even to test for their existence via the quality of fit tools.

Features		Labels or Targets	
t_j	$x_1^{j,i} = \pi_1 \circ \varphi_{\xi^i}(t_j)$	$\nu^{j,i} = \pi_2 \circ \varphi_{\xi^i}(t_j)$	$\mu^{j,i} = u_{\xi^i}(t_j)$
$t_0 = 0$	$x_1^{0,1}$	$\nu^{0,1}$	$\mu^{0,1}$
$t_0 = 0$	$x_1^{0,2}$	$\nu^{0,2}$	$\mu^{0,2}$
\vdots	\vdots	\vdots	\vdots
$t_0 = 0$	$x_1^{0,M}$	$\nu^{0,M}$	$\mu^{0,M}$
t_1	$x_1^{1,1}$	$\nu^{1,1}$	$\mu^{1,1}$
\vdots	\vdots	\vdots	\vdots
t_1	$x_1^{1,M}$	$\nu^{1,M}$	$\mu^{1,M}$
\vdots	\vdots	\vdots	\vdots
$t_N = T_p$	$x_1^{N,1}$	$\nu^{N,1}$	$\mu^{N,1}$
\vdots	\vdots	\vdots	\vdots
$t_N = T_p$	$x_1^{N,M}$	$\nu^{N,M}$	$\mu^{N,M}$

TABLE 3: Table showing a mapping between higher-level control objectives and their realization at a lower-level.

Outputs	Actuated Joints
Torso Pitch, Roll, and Yaw orientation	Stance Hip Pitch, Roll, and Yaw Joints
Stance Knee Joint	Stance Knee Joint
Swing Knee Joint	Swing Knee Joint
Stance Pitch Ankle Joint	Stance Pitch Ankle Joint
Stance Henke Ankle Joint	Stance Henke Ankle Joint
Swing Hip Pitch Joint	Swing Hip Pitch Joint
Swing Hip Roll Joint	Swing Hip Roll Joint
Swing Foot Pitch, Roll, and Yaw orientation	Swing Pitch and Henke Ankle Joints, and Swing Hip Yaw Joint

TABLE 4: Patient data. Selection criteria included being unable to stand by oneself, able to remain seated on a chair without further assistance, no ambulatory ability before using the exoskeleton, and low-to-moderate spasticity allowed.

Patient	Height(m)	Weight(kg)	Distance traveled(m)	speed(m/s)
A	1.80	68	8.9	0.11
B	1.69	80	10.56	0.15
C	1.80	75	9.5	0.13



Figure 1: ATALANTE: An exoskeleton designed by Wandercraft for people with paraplegia.

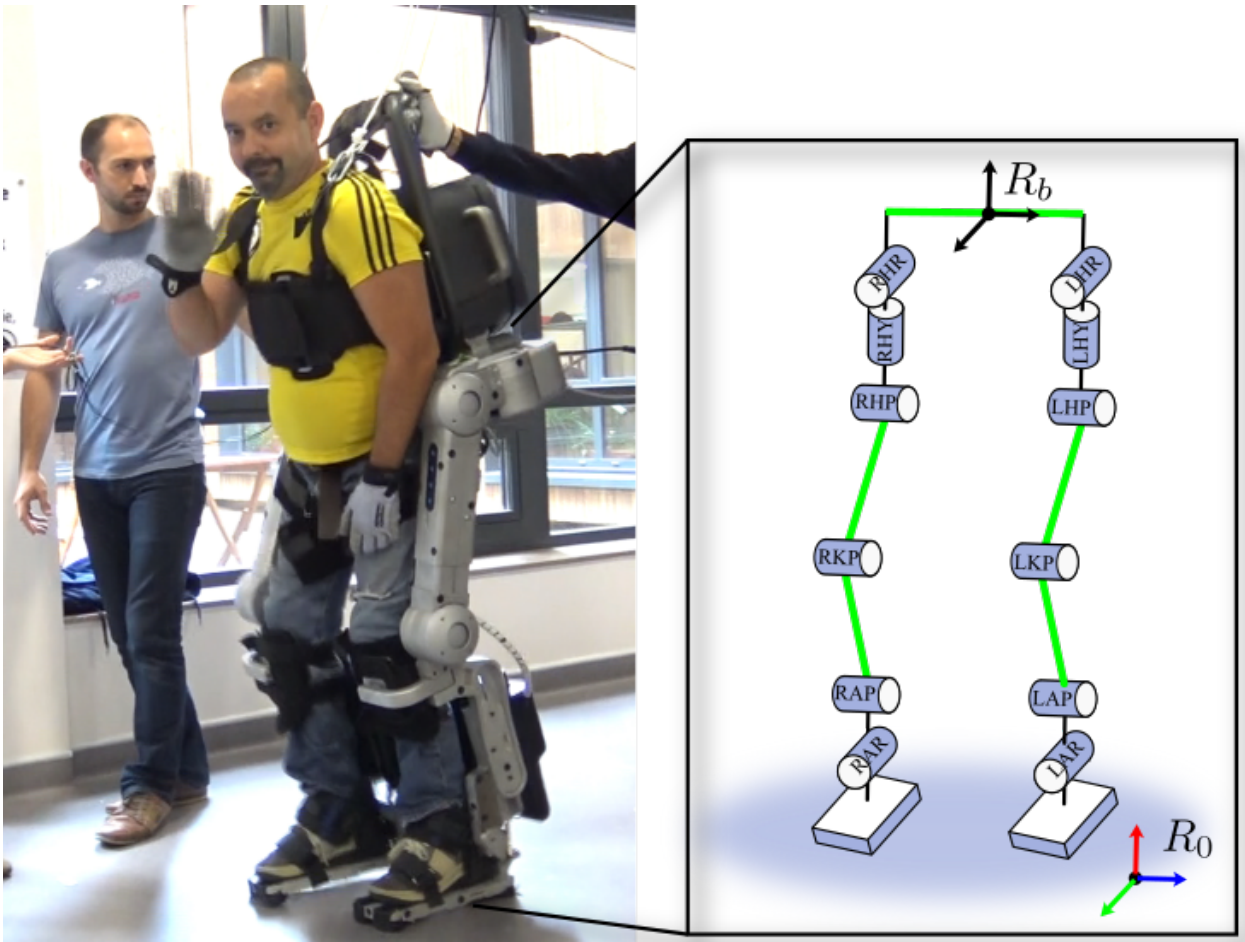


Figure 2: The kinematic diagram of human-exoskeleton lumped system. The patient is secured to the exoskeleton by means of fasteners located at the ankle, the shin, the thigh, the abdomen, and the torso. The lengths of links highlighted in green are adjustable.

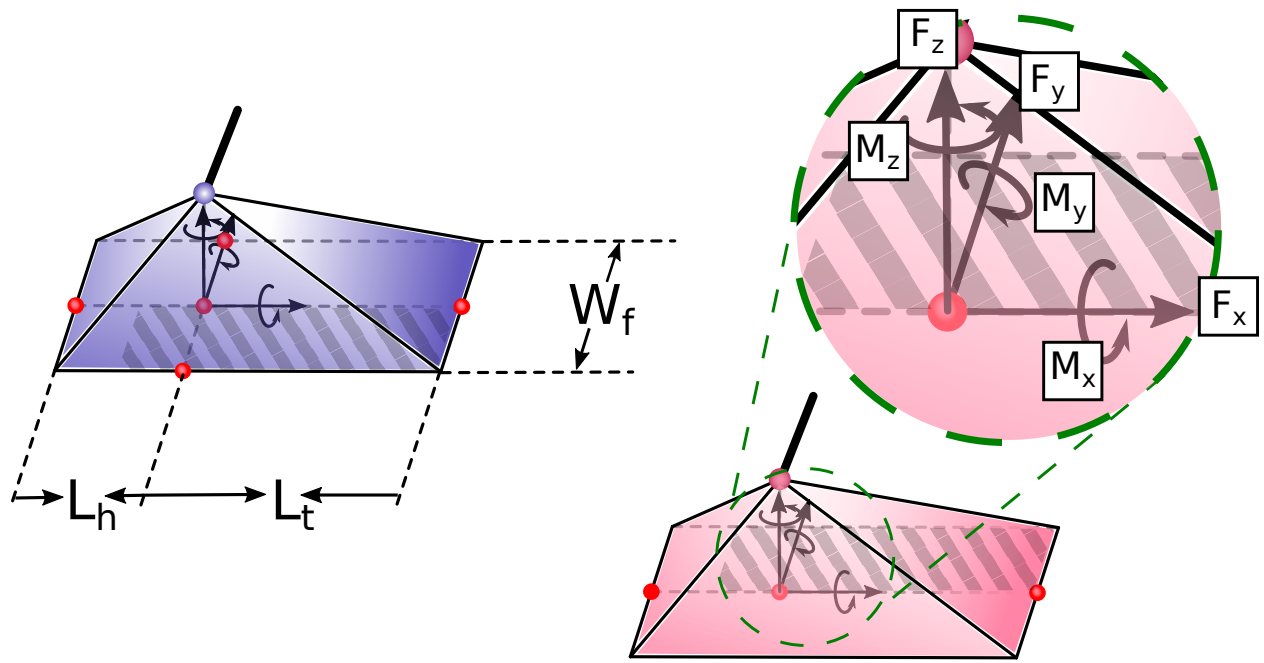


Figure 3: Depicts feet of the exoskeleton. Blue foot being the left while pink foot being the right. L_h and L_t denote the distance from the point of reference to the heel and toe respectively. W_f denotes the width of the foot. Shaded area depicts where the Zero Moment Point (ZMP) is desired to be in. $[F_x, F_y, F_z, M_x, M_y, M_z]$ is the resultant ground reaction force and moment acting on the foot during support, described in the body coordinate of the foot.

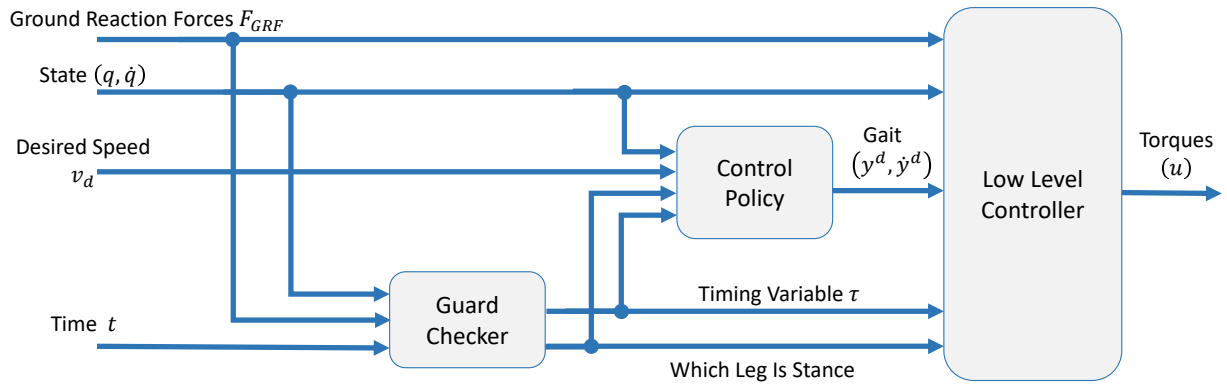


Figure 4: Overview of the controller structure used. Guard Checker handles detecting when to swap legs. Control Policy specifies the desired gait and the means to achieve it. The Low-level Controller translates control policy commands to desired joint-level trajectories and achieves them via PD control.

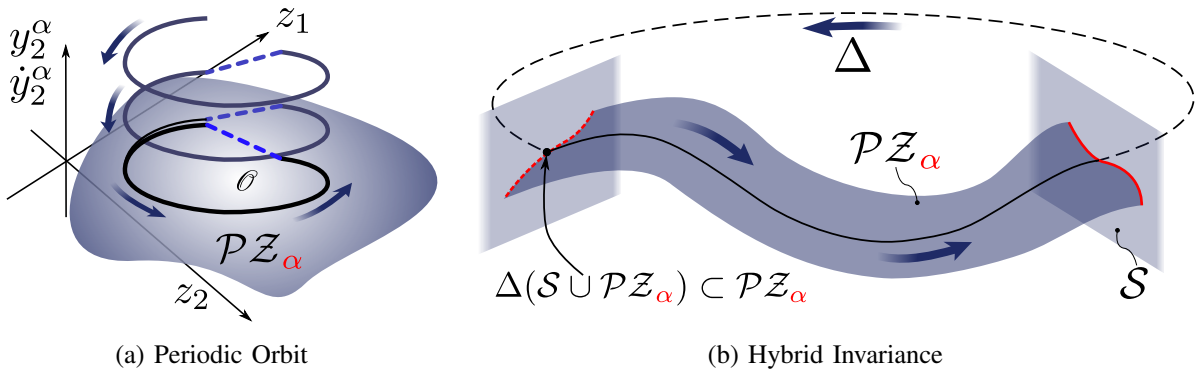


Figure 5: Illustration of a periodic orbit on the partial hybrid zero dynamics (PHZD) surface. A PHZD surface is constructed by choosing the proper parameters set α in the virtual constraints through optimization.

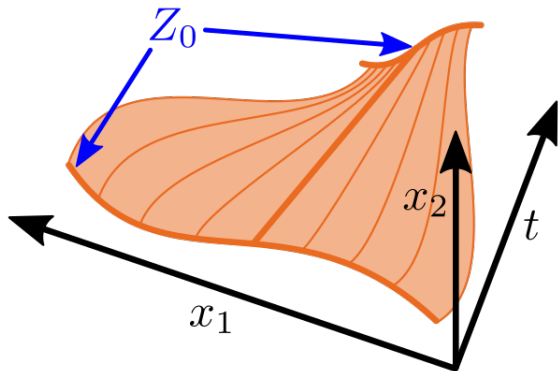


Figure 6: A collection of trajectories forming a smooth surface; while this is the desired outcome, it is not guaranteed. Direct-collocation-based optimization is used to design the trajectories.

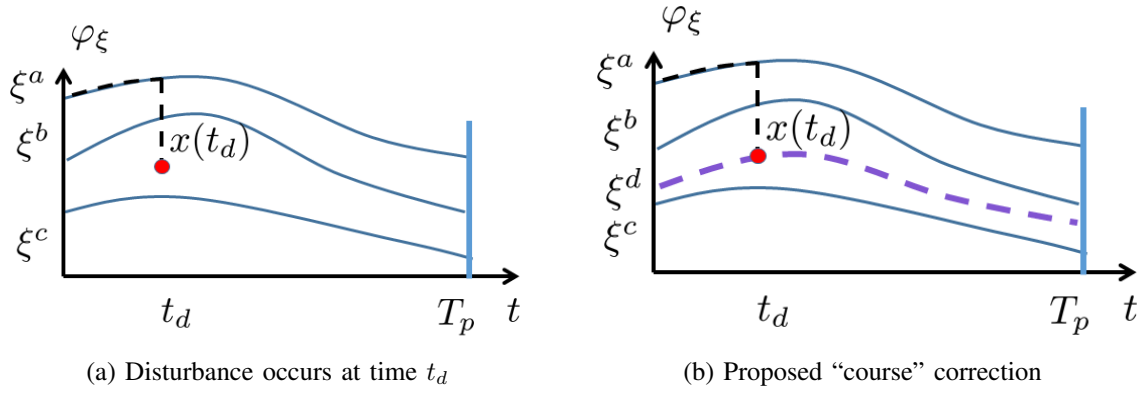


Figure 7: Gedanken Experiment. (a) Assume the system is initialized at ξ^a , with input, $u_{\xi^a}(t)$, being applied, and hence its solution is following $\varphi_{\xi^a}(t)$. Suppose that at time t_d , an “impulsive” disturbance instantaneously displaces the solution to a point $x(t_d)$. What input should be applied? (b) If there exists an $\xi^d \in Z_0$ such that $x(t_d) = \varphi_{\xi^d}(t_d)$, then applying the input $u_{\xi^d}(t)$ for $t_d \leq t < T_p$ will move the system toward the equilibrium in the sense that $\|\varphi_{\xi^d}(T_p) - \xi^*\| \leq c\|\xi^d - \xi^*\|$. This thought process leads to the “interpolation” or “learning” conditions in (17).

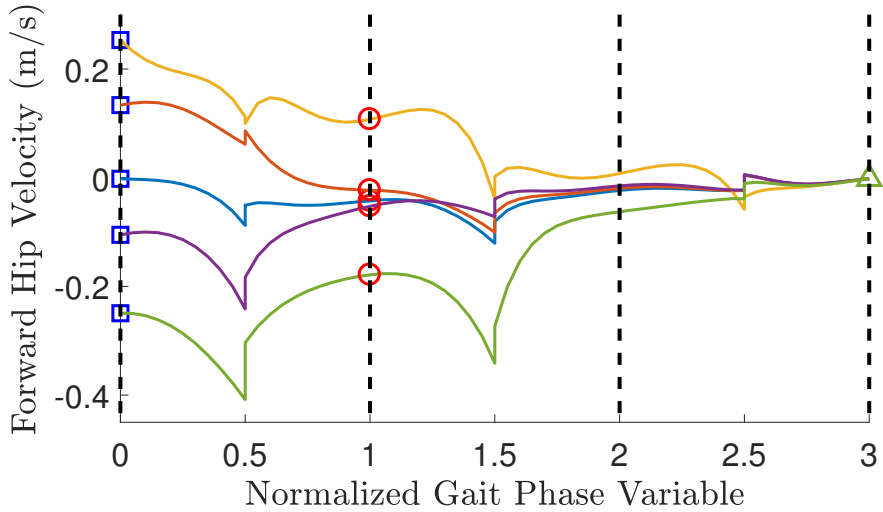


Figure 8: Shows forward velocity of the hip resulting from the transition optimizations. ~~Black dashed line marks the end of each step in the optimization.~~ Black vertical dashed lines marks the middle point of each step in the optimization, whereas the discontinuities in actual velocities between two dashed lines are due to the velocity changes from the rigid impact at the end of each step. Squares, circles, and the triangle mark points where the state of the system is in Z_0 . The blue squares mark starting states obtained from periodic gaits while the green triangle marks the ending desired state also obtained from a periodic gait. The red circles were made to be in Z_0 through an optimization constraint. The gait trajectory from the blue square to the red circle is what is used as training data for the Supervised Machine Learning.

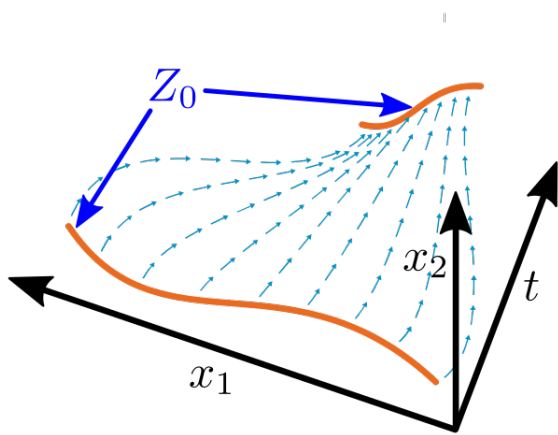


Figure 9: A vector field is constructed that gives rise to the trajectories, so it is a state-variable realization. Supervised Machine Learning (fancy regression) and model structure are used to “extract” the vector field from the trajectory optimization data.

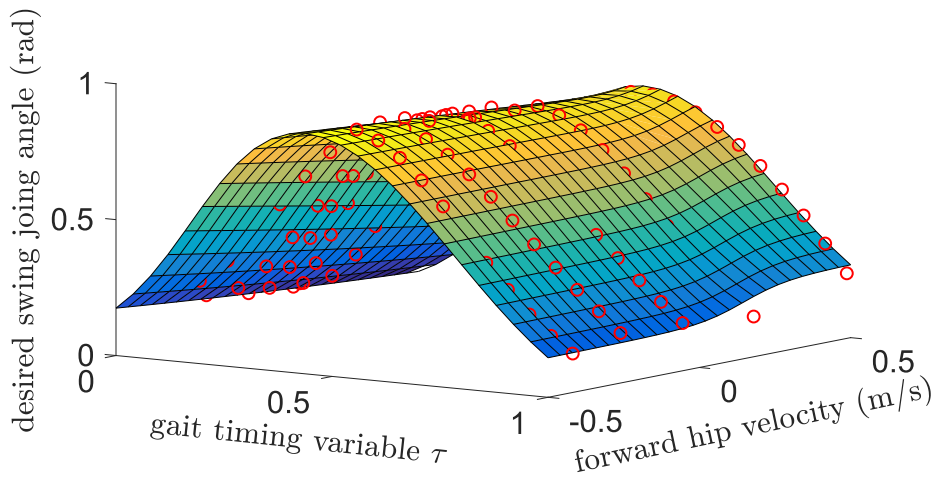


Figure 10: Surface showing the desired swing knee angle as a function of the gait timing variable τ and the forward hip velocity for stabilizing the step-in-place gait. The red circles are the actual data obtained from optimization while the surface is a regression done using the Neural Network Toolbox in MATLAB. Note that some of the circles are under the surface and are therefore not visible.

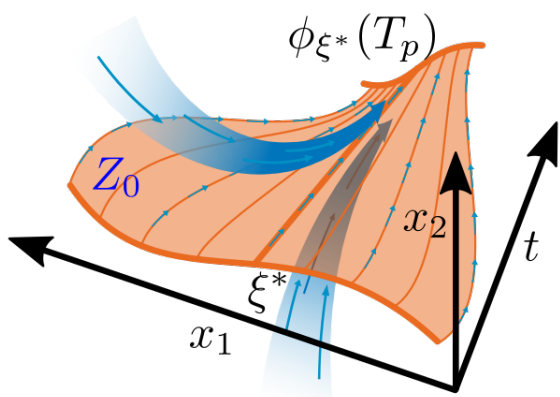


Figure 11: The low-dimensional realization (invariant surface and vector field) being rendered attractive in the full order model.

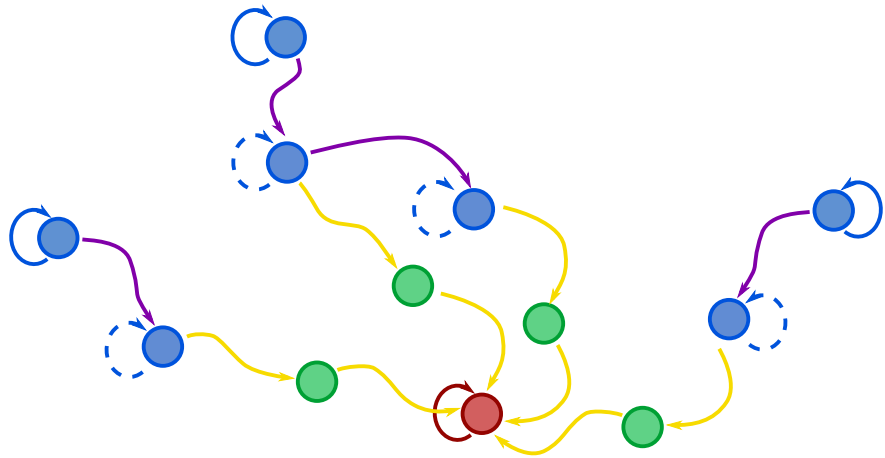


Figure 12: Graphical representation of gait optimization. Each arc represents one step of the exoskeleton. Circles with self-loops denote periodic orbits, while those without are transient states. The red circle denotes the goal (periodic) gait. The optimizations are done over three steps, with the end of the first step required to terminate in Z_0 , which is parameterized by periodic gaits, and the end of the third step must be the goal state. Since the first step initiates and ends in Z_0 , the three-step optimization can continue from the end of a first step and other self-loop-states in the same fashion as described above. The (first-step) trajectories corresponding to the time interval $[0, T_p]$ —denoted by the purple arcs—are saved and used as training data for the Supervised Machine Learning. The other data is discarded.

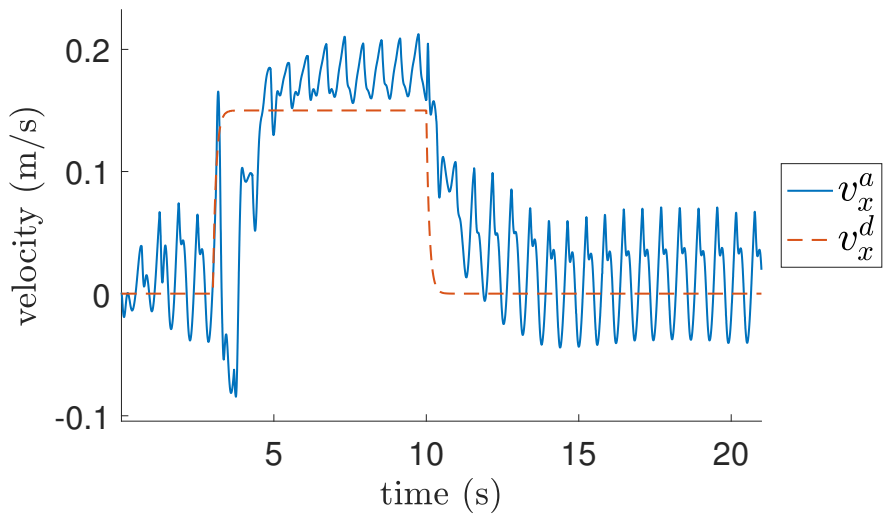


Figure 13: Shows tracking of a desired velocity profile. v_x^a is the actual forward velocity of the pelvis during walking. v_x^d is the commanded average forward velocity.

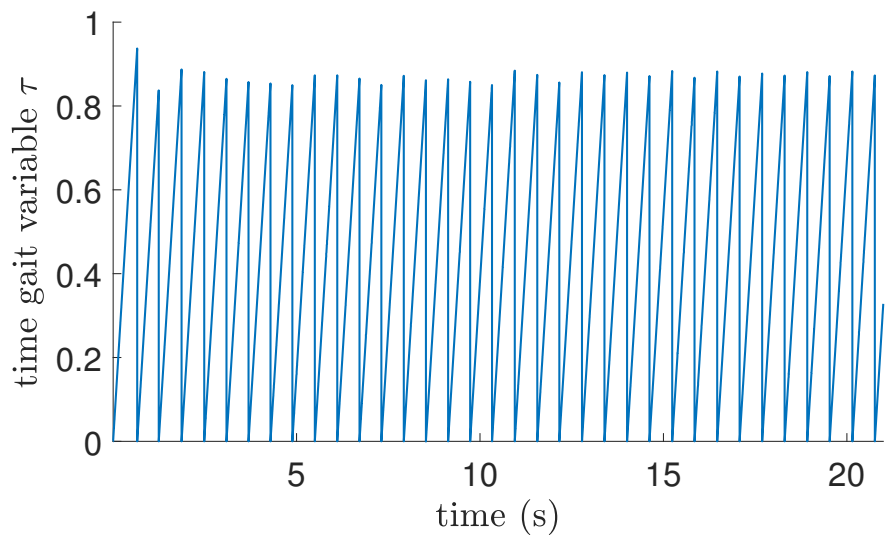


Figure 14: Shows the gait timing variable τ changing as a function of time while the exoskeleton was following a varying desired speed.

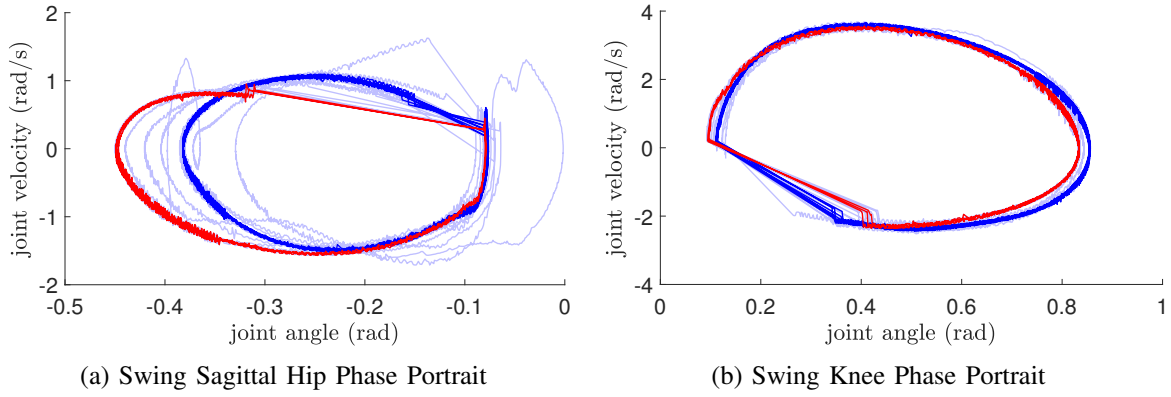


Figure 15: The phase portrait of both the swing and stance sagittal hip joints for when the system was tracking a desired velocity profile. Shows q vs \dot{q} for the two joints. The solid blue line shows the states at the last quarter of the simulation. While the solid red line shows the part of the simulation where the exoskeleton reached a steady state trajectory while walking forward. It can be seen that both cases, the exoskeleton converged to a periodic cycle.

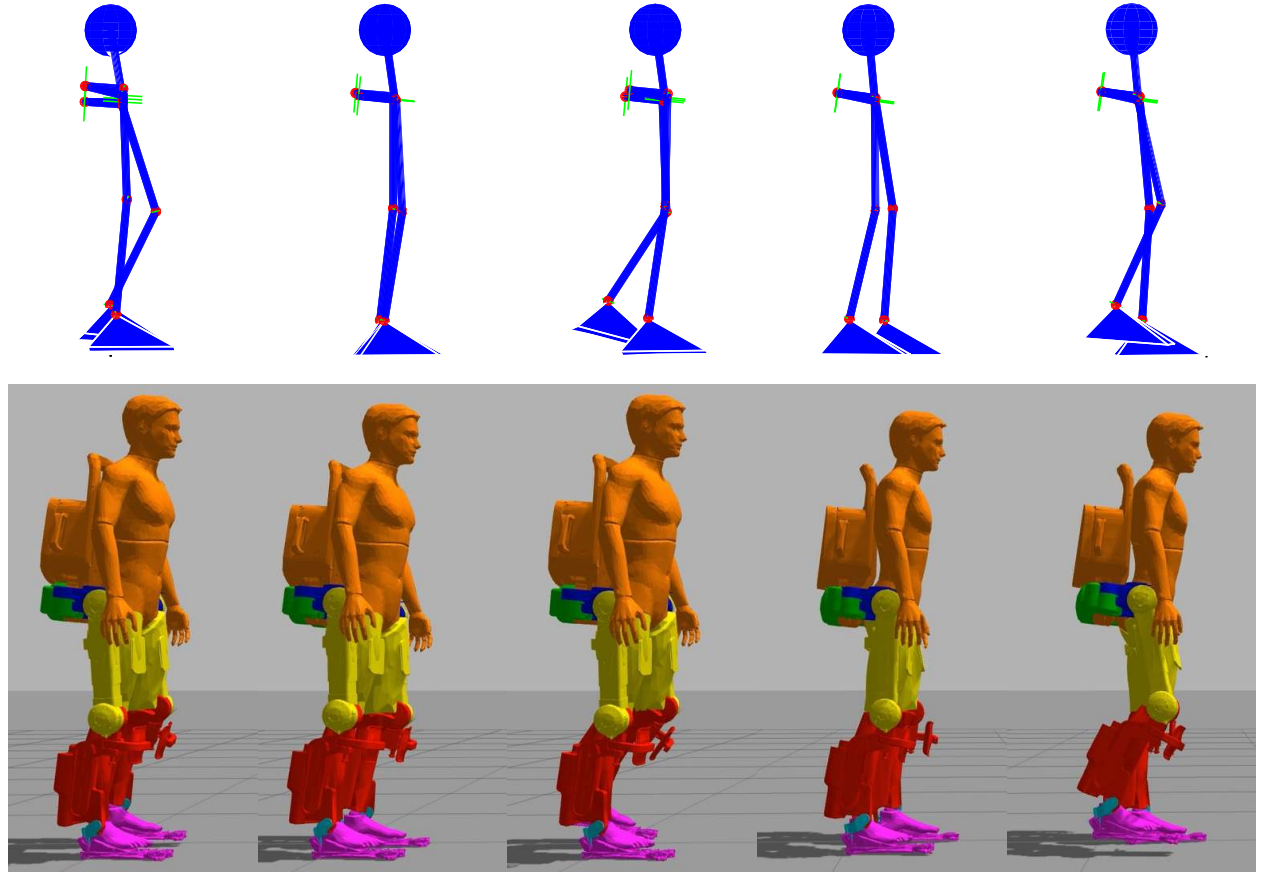
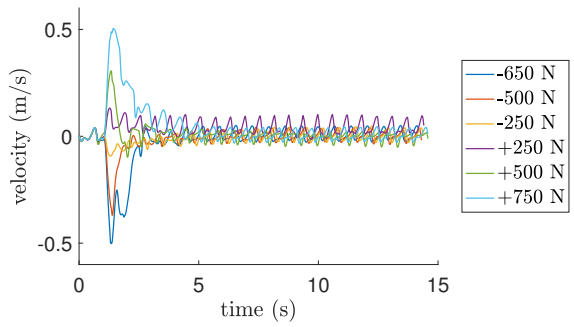
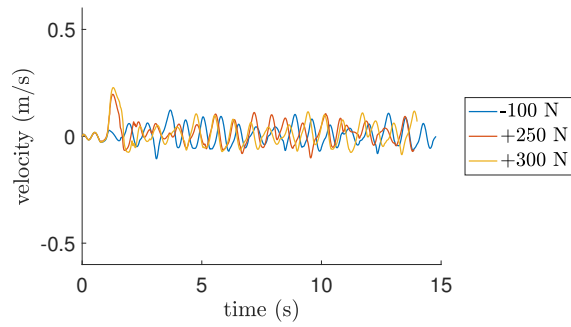


Figure 16: Displayed are the animations of the exoskeleton tracking a given desired velocity profile. Below are images from the Gazebo simulation, while above are stick figure with the same motion added for clarity. The first two photos show the step-in-place gait. The third image shows how the system looks like when it is starting to transition. The last two show the exoskeleton walking forward in a periodic gait.



(a) Supervised Machine Learning



(b) Fixed Gait

Figure 17: Change in hip velocity due to a perturbation. The control algorithm bases on Supervised Machine Learning was able to recover from much larger perturbations. Any larger perturbations on either controller resulted in falling.

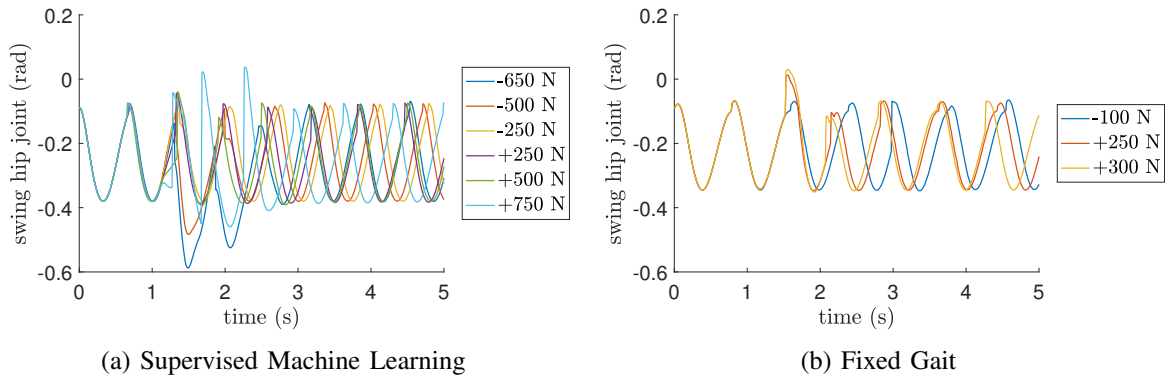


Figure 18: The swing hip joint angle as a function of time while responding to a perturbation. When experiencing large perturbations, the controller based on Supervised Machine Learning makes more use of its swing foot in order to return to a stepping-in-place gait.

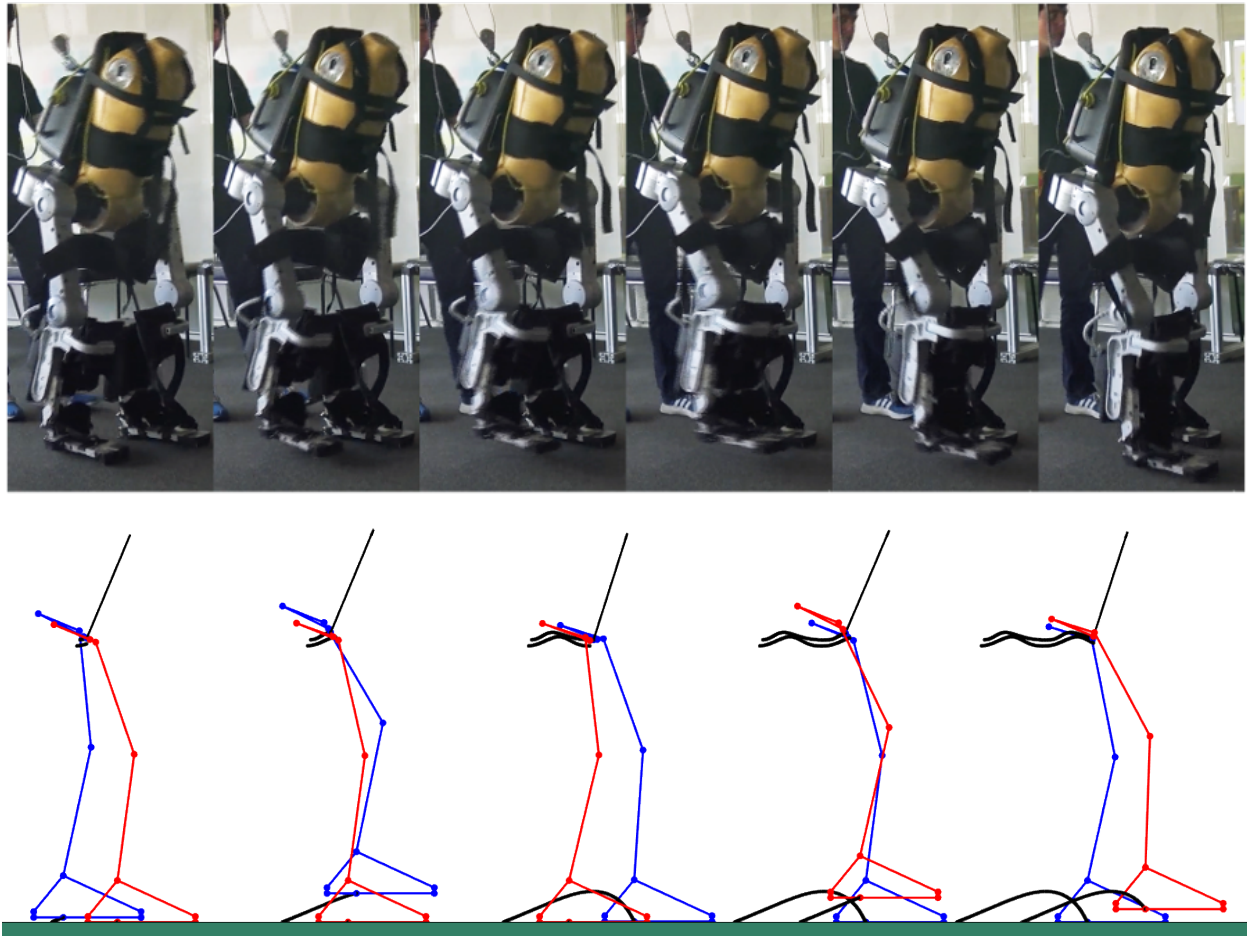


Figure 19: Tiled snapshot images of the nominal gait from the optimization for the exoskeleton with a mannequin inside in experiment and simulation. The black lines in the simulation images shows the evolution of the pelvis and the swing sole positions.

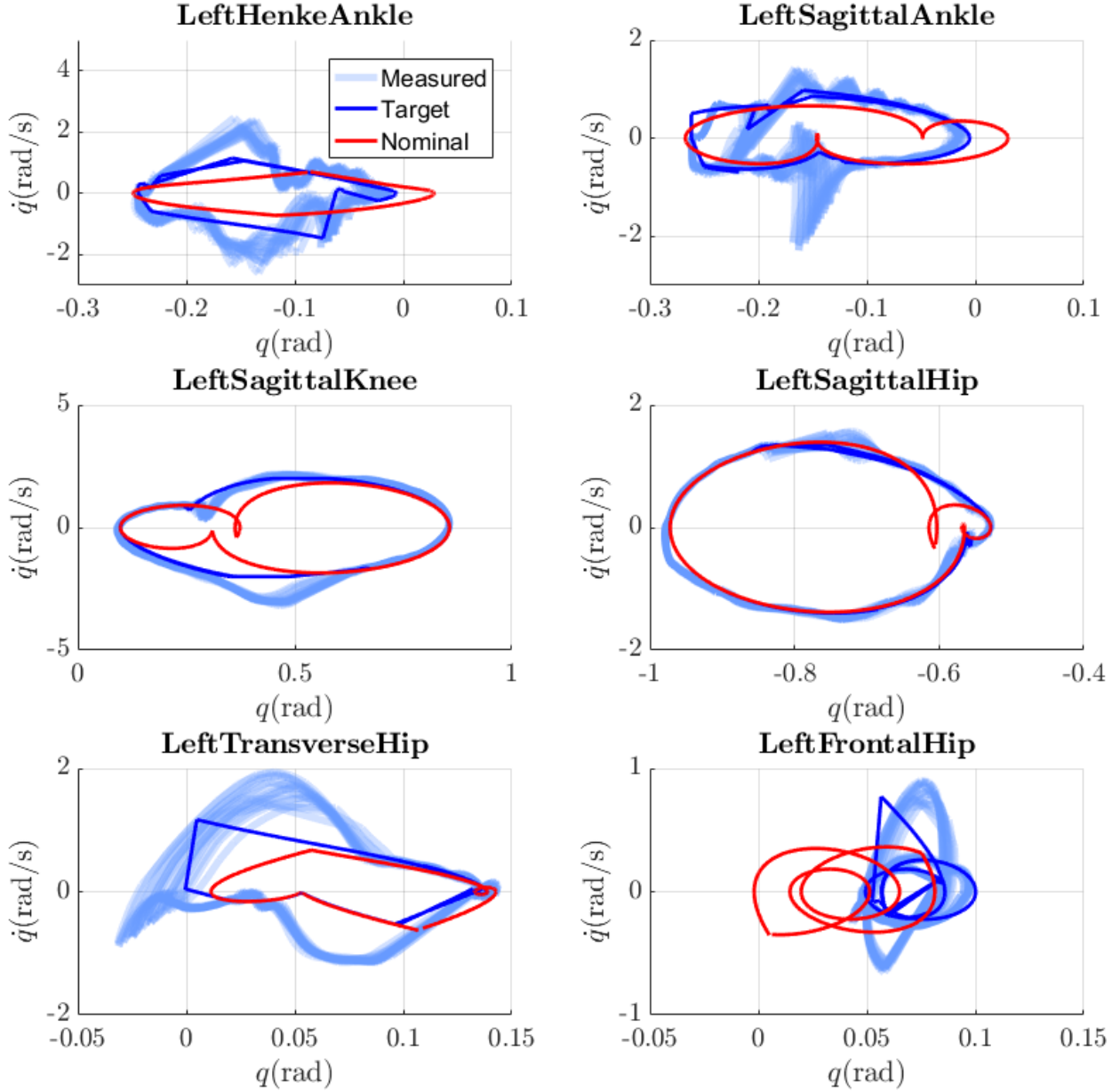


Figure 20: Phase portraits for the dummy during 20s of unassisted walking [54]. Red is the nominal orbit from optimization while blue is the “tuned” orbit to accommodate for mechanical imperfections and compliances of the robot.



Figure 21: From top to bottom, walking tiles of patients A, B and C.

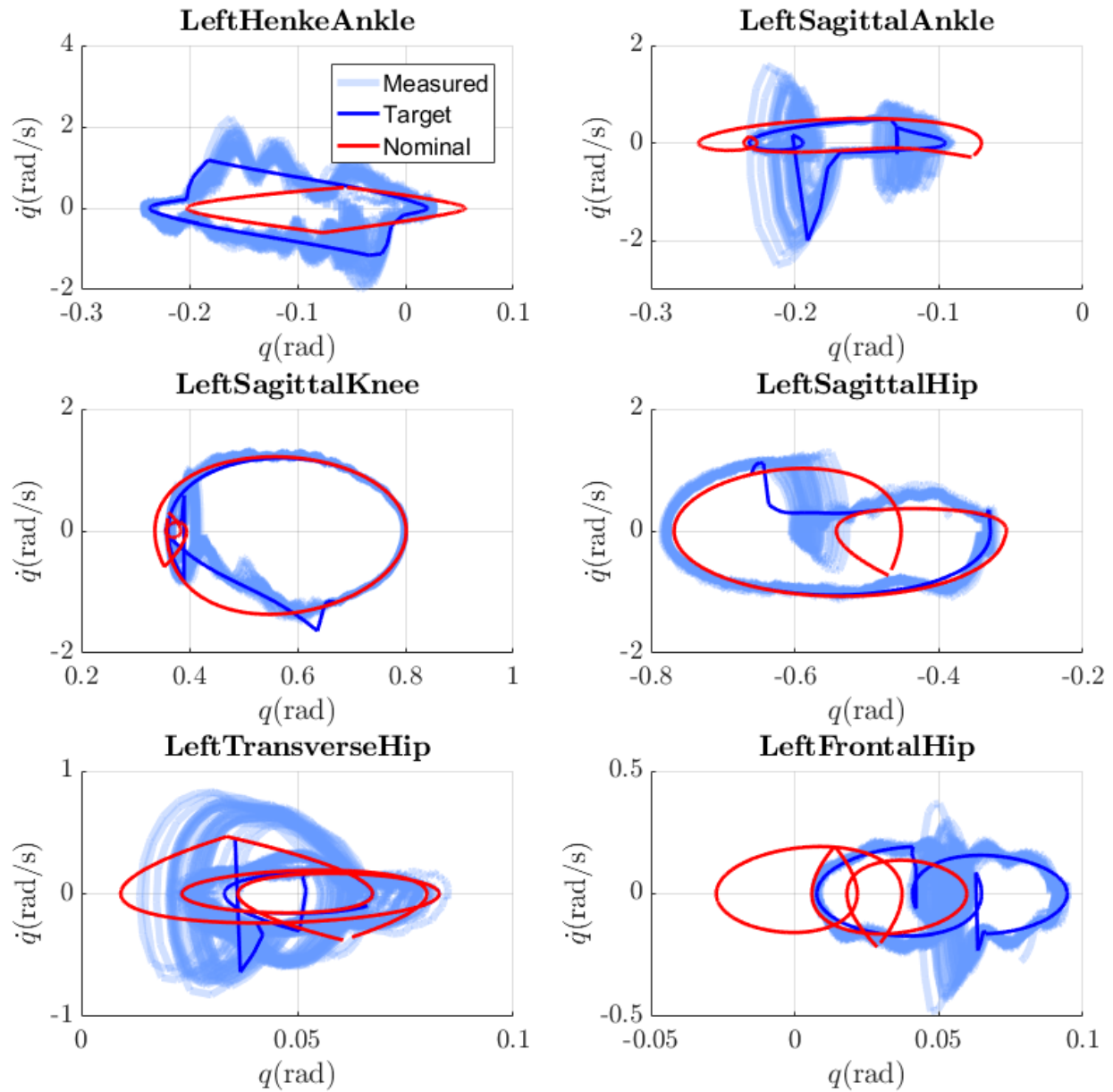


Figure 22: Phase portraits for patient A during 60s of unassisted walking.

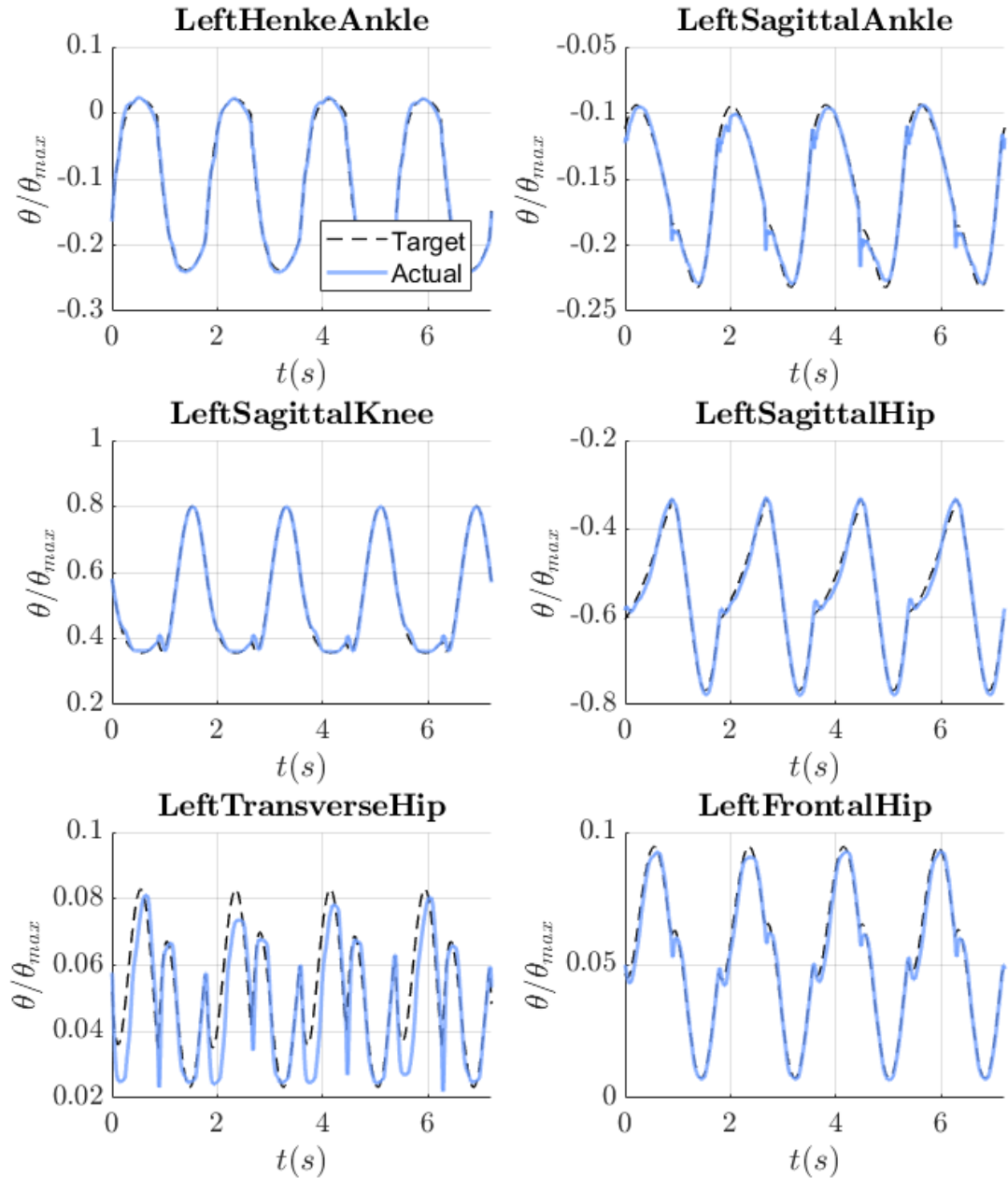


Figure 23: Selection of normalized tracking performance of the local controllers at the joint for patient A.

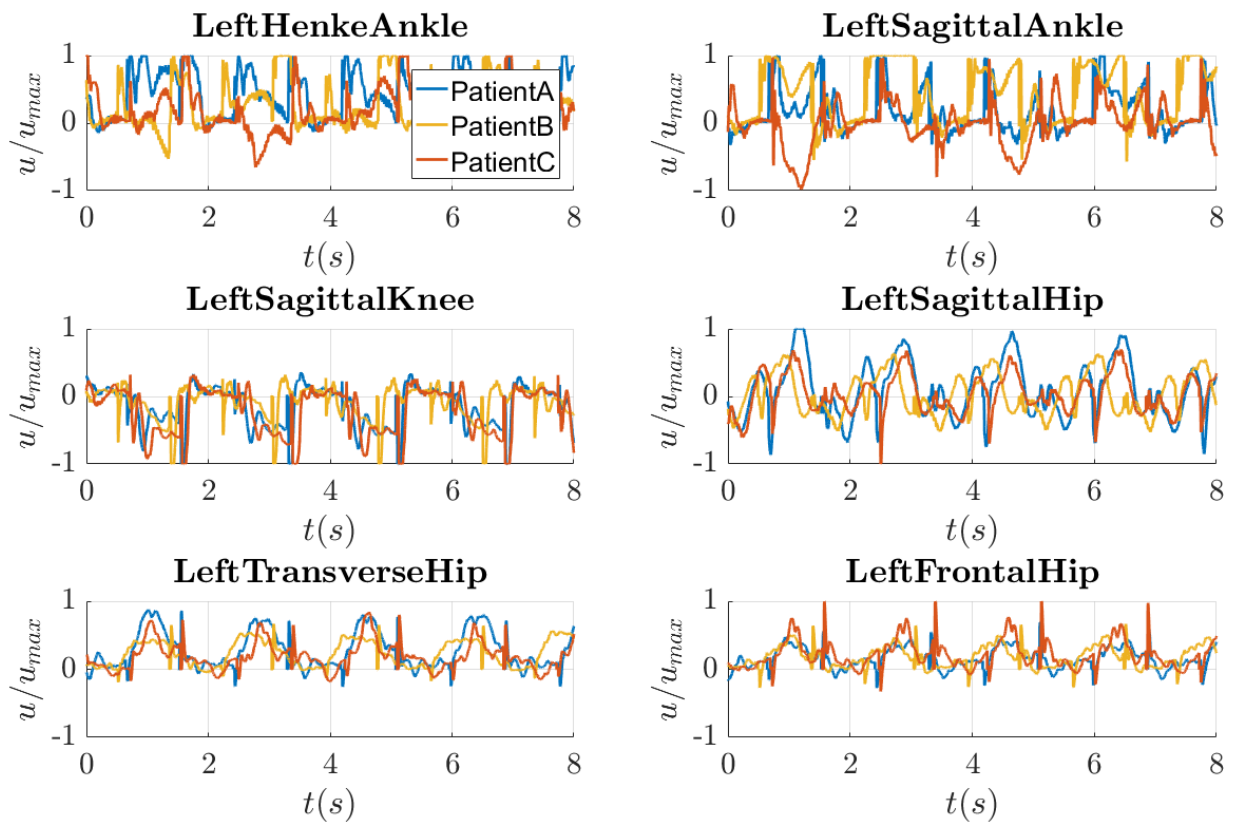


Figure 24: Normalized experimental motor torques for three different patients [54]. Other than for patient B, the motor torques rarely saturate. Hence there is reserve torque for responding to disturbances.

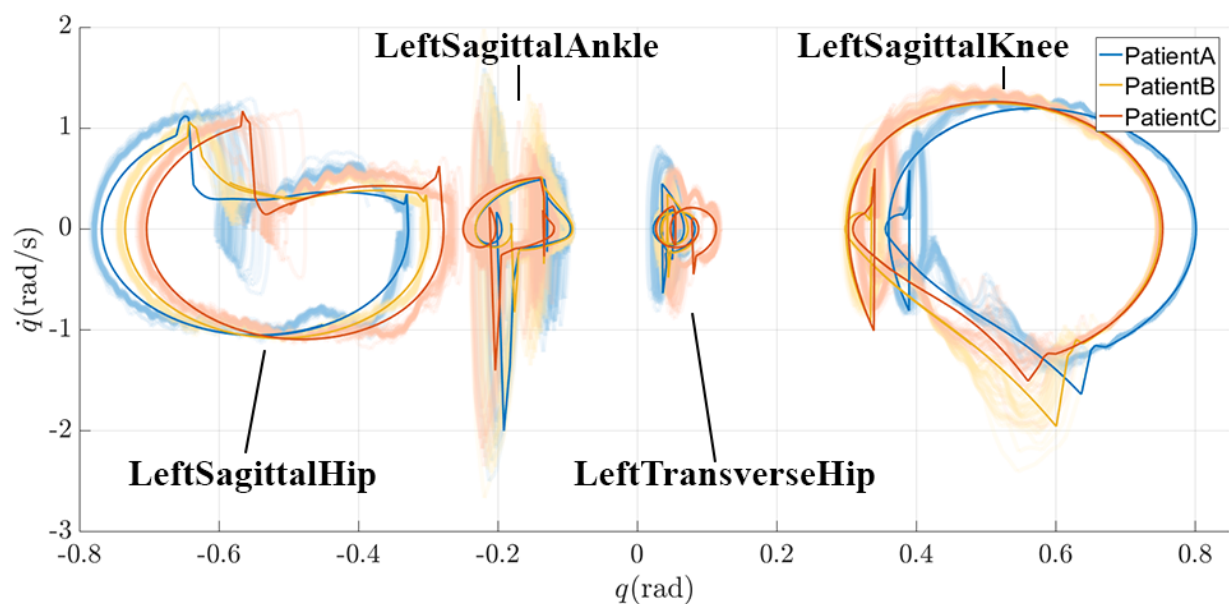


Figure 25: Selection of phase portraits. The solid lines are the target trajectories. The shaded regions are the measured joints positions.

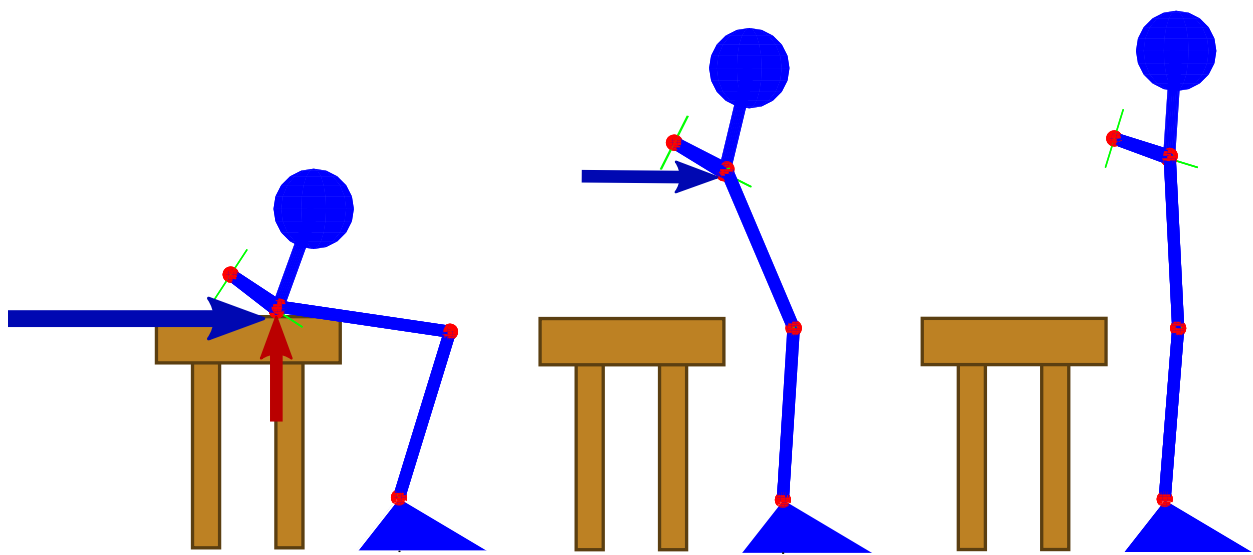


Figure 26: Stick figure animation of a user of the exoskeleton transitioning from sitting to standing. The first image is $t = 0$, the second image is $t = 0.6$ s, and the third image is $t = 1.8$ s. The blue and red arrows show external forces applied to the system through the user's arms. In the optimization, it is assumed that the user can exert up to half their body weight as an external force.

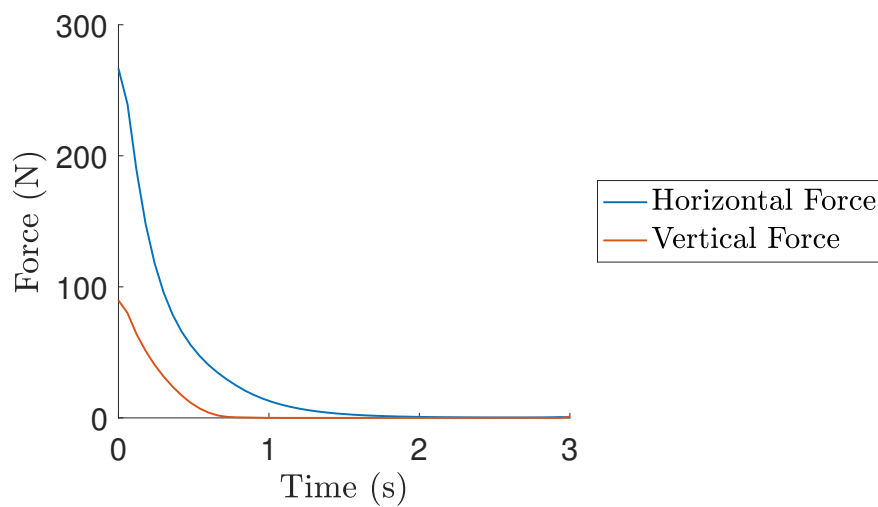


Figure 27: Force exerted by the user to assist in standing up. The exoskeleton is upright after 1.8 s from the start.

Sidebar: The Cybathlon

2 In October of 2016, ETH Zurich hosted a one-of-a-kind race for people with disabilities
4 using advanced assistive devices. The goal of the event was to enhance public awareness about
6 the challenges faced by people with disabilities. The event also served as a common platform for
8 biomechatronic devices **for** people with disabilities. A total of 66 pilots, 56 teams, 25 nations,
[S1].

10 The powered exoskeleton race was intended for participants with complete thoracic or
12 lumbar spinal cord injuries (SCI). Pilots, equipped with exoskeletons, were asked to complete as
14 many tasks as possible in a ten-minute time frame. These tasks were representative of common
16 day-to-day activities such as sitting on and standing up from a chair, walking around obstacles
[S1]. The German team, ReWalk, won first place, followed by IHMC from the United States,
and SG Mechatronics from Republic of Korea. The next Cybathlon is scheduled for May 2020.

18

References

- [S1] R. Riener and L. J. Seward. Cybathlon 2016. In *2014 IEEE International Conference on Systems, Man, and Cybernetics (SMC)*, pages 27922794, Oct 2014.
- [S2] Competition of cyborgs <http://multicle.news/> Accessed: 2018-01-28, Jan 2018.
- [S3] Cybathlon: Battle of the bionic athletes <http://www.bbc.com/news/technology-37605984> Accessed: 2018-01-28, Jan 2018.
- [S4] 2016 Cybathlon Powered Exoskeleton Race — SG Mechatronics. <https://youtu.be/KGHf5AWm3gs> Accessed: 2018-01-28, Jan 2018.
- [S5] Zurich: Cybathlon, la premire comptition de cyborgs en Suisse. <https://www.arcinfo.ch/articles/suisse/zurich-cybathlon-la-premiere-competition-de-cyborgs-de-suisse-587877> Accessed: 2018-01-28, Jan 2018.
- [S6] Final of the exoskeleton race at Cybathlon 2016 https://youtu.be/xq8c_hgMOZ8 Accessed: 2018-01-28, Jan 2018.
- [S7] Cyborg athlete goes for gold on robotic legs. <https://www.cnet.com/uk/news/cybathlon-athlete-mark-daniel-and-his-ihmc-robotic-exoskeleton/> Accessed: 2018-01-28, Jan 2018.



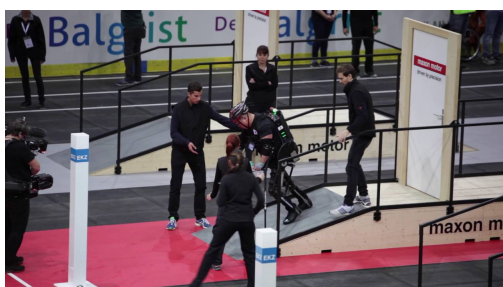
(a) The exoskeleton race arena at Cybathlon 2016. From: [S2]



(b) Sofa task. From: [S3]



(c) Slalom course. From: [S3]



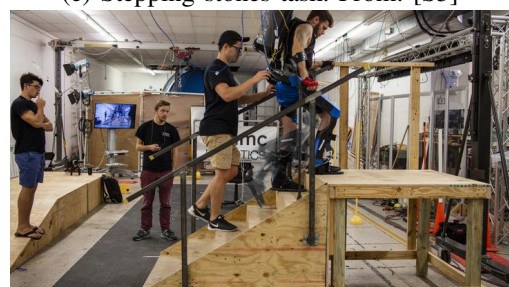
(d) Walking up ramps and through doorways. From: [S4]



(e) Stepping stones task. From: [S5]



(f) Walking across tilted paths. From: [S6]



(g) Walking over stairs. From: [S7]

Figure S1: Exoskeleton Race at Cybathlon 2016.

Sidebar: Pinned versus Floating base models

2 In Section The Exoskeleton and Its Dynamic Model, we use a set of floating base
3 coordinates, attached to the pelvis of the exoskeleton system, to describe the configuration of
4 the robot's base frame with respect to an inertial frame. The kinematic structure of the robot is
then built relative to the pelvis base frame, branching into swing and stance legs.

6 Another approach to describe the configuration of the robot is to use a *pinned* open chain
7 kinematic model [46]. In this approach, the robot's kinematic tree is built starting from the
8 stance foot and branching into the torso and swing leg. It is assumed that the stance foot is
9 attached to the ground through an ideal revolute joint. The advantage here is that the constraint
10 forces enforcing the holonomic constraints on the stance foot no longer appear in the resulting
equations of motion.

12 While the two models are equivalent, note however, that the position of the swing foot
13 with respect to the base frame (attached to the stance foot) in case of the pinned model involves
14 more trigonometric (sine and cosine) terms as compared to the floating base model, where the
base frame is attached to the pelvis. This is also reflected in the resulting equations of motion.
16 One consequence is that optimizations for finding periodic orbits run faster for the floating-base
model as compared to the pinned model.

Sidebar: How Direct Collocation Works

The direct collocation trajectory optimization utilizes the collocation methods for solving ordinary differential equations based on the finite step implicit Runge-Kutta methods [S1]. Here, the specific formulation of the Hermite-Simpson algorithm, one of the most commonly used direct collocation schemes, is introduced. Consider a system of the form $\dot{x} = f(x, u)$, a trajectory optimization problem for such system can be stated as

$$\begin{aligned} J(x(t), u(t)) &= \min_{u(t)} \quad \int_0^T L(x(t), u(t)) dt \\ \text{st. } x(t) &= \int_0^t f(x(t), u(t)) dt \\ &\quad 0 \geq c(x(t), u(t)), \quad 0 \leq t \leq T, \end{aligned} \tag{S1}$$

- ² where $L(\cdot)$ represent the running cost function, and $c(\cdot)$ represents the path constraints.
- To solve this problem using direct collocation, a discrete representation of the continuous time solution is introduced.
- Specifically, the time interval $t \in [0, T]$ is divided into a fixed number of uniformly distributed intervals (see Figure S2). In particular, the even-numbered nodes (e.g., t_0, t_2, \dots, t_N) are called cardinal nodes, and the odd-numbered nodes between every two cardinal nodes are called interior nodes.
- At each discrete node of $t = t_i$, an approximation of state variables $x_i = x(t_i)$ and control inputs $u_i = u(t_i)$ is introduced as a set of optimization variables to be solved.
- In this paper, the approximation of the slope of state variables $\dot{x}_i = \dot{x}(t_i)$ is also introduced as *defect variables* in the optimization.

The Hermite-Simpson methods then use piece-wise continuous cubic interpolation polynomials to approximate the solution of the system over each interval between two neighboring cardinal nodes. This approximation can be fully determined by the approximated state variables and slopes at the cardinal nodes. Hence, if the approximated states x_i and slopes \dot{x}_i at the interior nodes match the interpolation polynomial at time $t = t_i$ (e.g., \bar{x}_i and $\dot{\bar{x}}_i$ in Figure S2), then the resulting piece-wise polynomials are considered as an approximated solution of the system [S2]. To find this approximated solution, e.g., the discrete representation of the states, the original continuous time trajectory optimization problem can be converted to the following form given

by

$$\begin{aligned} J(x_i, u_i) = \min_{u_i} \quad & \sum_{i=1}^{N-1} w_i L(x_i, u_i) \\ \text{st. } \quad & \dot{x}_i = f(x_i, u_i) \\ & c(x_i, u_i) \geq 0, \quad 0 \leq i \leq N \\ & \dot{x}_i - 3(x_{i+1} - x_{i-1})/2\Delta t_i + (\dot{x}_{i-1} + \dot{x}_{i+1})/4 = 0 \\ & x_i - (x_{i+1} + x_{i-1})/2 - \Delta t_i(\dot{x}_{i-1} - \dot{x}_{i+1})/8 = 0, \end{aligned} \tag{S2}$$

where for all $i \in \{1, 3, \dots, N-1\}$, where $\Delta t_i = t_{i+1} - t_{i-1}$ is the time interval between two cardinal nodes, and w_i is weighting factor of each node determined by the Gaussian quadrature [50]. Specifically, the last two constraints are called *collocation constraints*, which are determined by cubic interpolation polynomials. The above nonlinear programming problem can be solved straightforwardly by existing numerical NLP solvers.

6

References

- [S1] John T Betts. Survey of numerical methods for trajectory optimization. *Journal of guidance, control, and dynamics*, 21(2):193207, 1998.
- [S2] Charles R Hargraves and Stephen W Paris. Direct trajectory optimization using nonlinear programming and collocation. *Journal of Guidance, Control, and Dynamics*, 10(4):338 342, 1987.

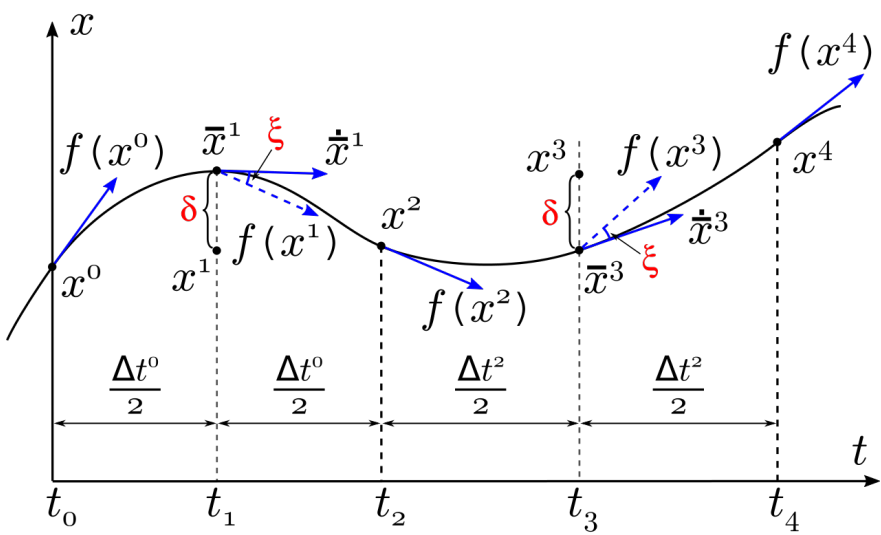


Figure S2: Illustration of defect constraints and node distribution of the direct collocation optimization [50].

Author Biography

Omar Harib (Corresponding Author, oharib@umich.edu) is a Ph.D. candidate in Electrical and Computer Engineering at the University of Michigan, Ann Arbor. He double majored and earned bachelor degrees in both Mechanical Engineering and Computer Engineering at the American University of Sharjah, UAE. His current research interests are in control theory and experimentation focusing on bipedal robot locomotion.

Ayonga Hereid received the Ph.D. in Mechanical Engineering from the Georgia Institute of Technology in 2016. He is currently a postdoctoral research fellow at the department of Electrical Engineering and Computer Science at the University of Michigan. He received the DENSO Best Student Paper Award of the 17th International Conference on Hybrid System: Computation and Control in 2014. His current research interests center around developing advanced nonlinear optimization and control algorithms to realize dynamic and natural locomotion on bipedal robots.

Ayush Agrawal received an M.S. degree in Mechanical Engineering from Carnegie Mellon University, Pittsburgh in 2017 and a B.Tech degree in Mechanical Engineering from the National Institute of Technology, Karnataka, India in 2015. He is currently a Ph.D. student in the Department of Mechanical Engineering at UC Berkeley and is part of the Hybrid Robotics Lab. His research interests are in the areas of nonlinear control and bipedal locomotion.

Thomas Gurriet graduated from Arts et Mtiens ParisTech and Georgia Institute of technology with a M.S. in Mechanical Engineering in 2015. He is currently pursuing a Ph.D. degree in the the Department of Mechanical and Civil Engineering at the California Institute of Technology. His current research interests are in Safety Critical Control.

Sylvain Finet graduated from ENSTA ParisTech in 2013 and completed a PhD in bipedal robotic at Mines ParisTech in 2017. He joined Wandercraft from its very beginnings, where he is working as a control engineer. His current research interests include theoretical and experimental aspects of nonlinear control and bipedal robotic.

Guilhem Boris graduated from Ecole Polytechnique in 2011 and completed a Master of Science in Theoretical Physics at Ecole Normale Suprieure de Paris in 2012. He worked as a PhD student on quantum Monte Carlo methods to study superfluid phase transitions in disordered Bose gases. He is presently working as a control engineer at Wandercraft. His current research interests include theoretical and experimental aspects of nonlinear control and bipedal locomotion.

Alexis Duburcq is a Ph.D student in Robotics and Computer Engineering at the University of Dauphine, Paris France. He received an M.S. degree in Microengineering from Ecole

Polytechnique Fdrale de Lausanne in 2017 and he graduated from the Ecole Centrale Paris in
2 2017. He joined Wandercraft in January 2017, where he is working on HZD Gait Optimization.
His current research interests are in Machine Learning applied to locomotion for exoskeletons.

4 **Eva Mungai** received her bachelor degree in Mechanical Engineering at Rensselaer
Polytechnic Institute in 2017. She is currently pursuing her M.S. and Ph.D in Mechanical
6 Engineering at the University of Michigan, Ann Arbor. Her current research interests are in
implementing control theory for bipedal locomotion and the task of standing and sitting for
8 biped robots.

10 **Matthieu Masselin** graduated from both the Ecole Polytechnique and Kungliga Tekniska
Hgskolan (KTH) of Stockholm in 2013 where he completed a Master of Science in Electro-
Physics. He quickly joined Wandercraft after where he has since been developing the control
12 team. He has lead an effort to implement dynamic walking on Wandercraft exoskeleton, building
on knowledge developed for biped robots.

14 **Aaron D. Ames** is the Bren Professor of Mechanical and Civil Engineering and Control
and Dynamical Systems at Caltech. Prior to joining Caltech in 2017, he was an Associate
16 Professor at Georgia Tech in the Woodruff School of Mechanical Engineering and the School of
Electrical & Computer Engineering. He received a B.S. in Mechanical Engineering and a B.A. in
18 Mathematics from the University of St. Thomas in 2001, and he received a M.A. in Mathematics
and a Ph.D. in Electrical Engineering and Computer Sciences from UC Berkeley in 2006. He
20 served as a Postdoctoral Scholar in Control and Dynamical Systems at Caltech from 2006 to
2008, and began is faculty career at Texas A&M University in 2008. At UC Berkeley, he was the
22 recipient of the 2005 Leon O. Chua Award for achievement in nonlinear science and the 2006
Bernard Friedman Memorial Prize in Applied Mathematics, and he received the NSF CAREER
24 award in 2010 and the 2015 Donald P. Eckman Award. His research interests span the areas of
robotics, nonlinear control and hybrid systems, with a special focus on applications to bipedal
26 robotic walkingboth formally and through experimental validation. His lab designs, builds and
tests novel bipedal robots, humanoids and prostheses with the goal of achieving human-like
28 bipedal robotic locomotion and translating these capabilities to robotic assistive devices.

30 **Koushil Sreenath** is an Assistant Professor of Mechanical Engineering, at UC Berkeley.
He received a Ph.D. degree in Electrical Engineering and Computer Science and a M.S. degree
in Applied Mathematics from the University of Michigan at Ann Arbor, MI, in 2011. He was a
32 Postdoctoral Scholar at the GRASP Lab at University of Pennsylvania from 2011 to 2013 and
an Assistant Professor at Carnegie Mellon University from 2013 to 2017. His research interest
34 lies at the intersection of highly dynamic robotics and applied nonlinear control. He received

the Best Paper Award at the Robotics: Science and Systems (RSS) Conference in 2013, and the
2 Google Faculty Research Award in Robotics in 2015.

4 **Jessy W. Grizzle** is the Director of Michigan Robotics. He received the Ph.D. in electrical
engineering from The University of Texas at Austin in 1983. He is currently a Professor of
6 Electrical Engineering and Computer Science at the University of Michigan, where he holds the
titles of the Elmer Gilbert Distinguished University Professor and the Jerry and Carol Levin
Professor of Engineering. He jointly holds sixteen patents dealing with emissions reduction in
8 passenger vehicles through improved control system design. Professor Grizzle is a Fellow of the
IEEE and IFAC. He received the Paper of the Year Award from the IEEE Vehicular Technology
10 Society in 1993, the George S. Axelby Award in 2002, the Control Systems Technology Award
in 2003, the Bode Prize in 2012 and the IEEE Transactions on Control Systems Technology
12 Outstanding Paper Award in 2014. His work on bipedal locomotion has been the object of
numerous plenary lectures and has been featured on CNN, ESPN, Discovery Channel, The
14 Economist, Wired Magazine, Discover Magazine, Scientific American and Popular Mechanics.